Investigating the Impact of LncRNAs PUNISHER and GAS5 on the Pathogenesis of Calcific Aortic Valve Disease

Dissertation

zur Erlangung des Doktorgrades (Dr. med.)

der Medizinischen Fakultät

der Rheinischen Friedrich-Wilhelms-Universität

Bonn

Yuan Zhou

aus Anhui, China

2025

Angefertigt mit der Genehmigung

der Medizinischen Fakultät der Universität Bonn

1. Gutachter: PD Dr. med. Felix Jansen

2. Gutachter: Prof. Dr. Wilhelm Röll

Tag der mündlichen Prüfung: 26.06.2025

Aus der Medizinischen Klinik II - Innere Medizin (Kardiologie, Pneumologie)

Table of Contents

List of abbreviations 6

1.Introduction 8

1.1 Background on Calcific Aortic Valvular Disease - CAVD 8

1.2 Role of Long Non-Coding RNAs in Cardiovascular Diseases 11

1.3 Biological Significance of PUNISHER and GAS5 12

1.4 Aims of the study 13

2. Materials and Methods 15

2.1 Materials 15

2.2 Methods 19

2.2.1 Cell Culture 19

2.2.2 Transfection Procedures 20

2.2.3 In vitro EndMT Induction in HCAECs 20

2.2.4 In vitro Calcification Induction in HCASMCs and VICs 21

2.2.5 RNA isolation and qRT-PCR 22

2.2.6 MTT Assay on VICs 22

2.2.7 Proliferation Assessment via BRDU Incorporation 22

2.2.8 Immunofluorescence Staining 23

2.2.9 Western Blot 23

2.2.10 Apoptosis Protein Array Analysis of Calcification-induced Transfected VICs 25

2.2.11 TaqMan Array Human Osteogenesis Analysis of Calcification-induced Transfected VICs 25

2.2.12 Statistical Analysis 26

3. Results 27

3.1 Impact of lncRNAs Dysregulation on Endothelial-to-Mesenchymal Transition (EndMT) in HCAECs 27

3.1.1 PUNISHER Expression changes in HCAECs: 27

3.1.2 GAS5 Expression changes in HCAECs: 27

3.1.3 Knockdown of PUNISHER and GAS5 in HCAECs: 27

3.1.4 RT-qPCR Analysis of EndMT Markers (ACTA2 and VMF): 27

3.1.5 Morphological Changes in HCAECs Post-EndMT: 29

3.1.6 Cell Migration Assays Post-Knockdown 29

3.1.7 Western Blot Analysis of EndMT-Related Proteins (CD31, VEGFA, ALPL, Vimentin) 29

3.2 Influence of PUNISHER and GAS5 on Calcification Processes in HCASMCs 31

3.2.1 Altered Expression of PUNISHER and GAS5 in HCASMCs Under Calcification Stimulation 31

3.2.2 Assessment of Calcification Markers in HCASMCs Post-Knockdown and Calcification Stimulation 31

3.2.3 Western Blot Analysis of Calcification Markers Post-Knockdown 32

3.2.4 Impact of PUNISHER and GAS5 Knockdown on Cell Migration and Proliferation 32

3.3 Role of PUNISHER and GAS5 in VIC Calcification 34

3.3.1 Expression of PUNISHER and GAS5 in VICs Post-Calcification 34

3.3.3 Assessment of Calcification Markers in VICs Post-Knockdown and Calcification Stimulation 35

3.3.4 Western Blot Analysis of Calcification Markers Post-Knockdown 35

3.3.5 MTT Assay on VICs Post-Treatment 35

3.3.6 Proliferation Assessment via BRDU Incorporation 35

3.4 Molecular Effects of LncRNA Modulation in VICs 38

3.4.1 Differential Gene Expression Post-LncRNA Knockdown and Calcification Treatment 38

3.4.2 Apoptotic Response to LncRNA Knockdown in VICs 42

4. Discussion 49

5. Summary 55

6. List of Figures 57

7. List of Tables 58

8. References 59

9. Acknowledgments 67

List of abbreviations

ACTA2	Actin Alpha 2
ALPL	Alkaline Phosphatase, Liver/Bone/Kidney
BMP2	Bone Morphogenetic Protein 2
BrdU	Bromodeoxyuridine
CAVD	Calcific Aortic Valvular Disease
CMs	Cardiomyocytes
CVDs	Cardiovascular diseases
DAPI	4',6-Diamidino-2-Phenylindole
DMEM	Dulbecco's Modified Eagle Medium
ECs	Endothelial Cells
ECL	Enhanced Chemiluminescence
EndMT	Endothelial-to-Mesenchymal Transition
EVs	Extracellular Vesicles
FBS	Fetal Bovine Serum
GAPDH	Glyceraldehyde-3-Phosphate Dehydrogenase
GAS5	Long-Non-Coding RNA Growth Arrest-Specific 5
HCASMCs	Human Coronary Artery Smooth Muscle Cells
HCAECs	Human Coronary Artery Endothelial Cells
HCL	Hydrochloric Acid
HIF1-α	Hypoxia-Inducible Factor 1-Alpha
HnRNPK	Heterogeneous Nuclear Ribonucleoprotein K
HnRNPU	Heterogeneous Nuclear Ribonucleoprotein U
IL1β	Interleukin-1 Beta
LVEF	Left Ventricular Ejection Fraction
MGP	Matrix Gla Protein
MVs	Microvesicles
NOS3	Nitric Oxide Synthase 3
PECAM	Platelet And Endothelial Cell Adhesion Molecule
PFA	Paraformaldehyde
PUNISHER	Long Non-Coding RNA PUNISHER

qRT-PCR	Quantitative Reverse Transcription Polymerase Chain Reaction
RANKL	Receptor Activator of Nuclear Factor Kappa-B Ligand
RNAiMAX	Lipofectamine RNAiMAX
RUNX2	Runt-Related Transcription Factor 2
siRNA	Small Interfering RNA
SMCs	Smooth Muscle Cells
TAVR	Transcatheter Aortic Valve Replacement
TGFβ1	Transforming Growth Factor Beta 1
TNF-α	Tumor Necrosis Factor Alpha
TRIzol	TRIzol Reagent
VECs	Valvular Endothelial Cells
VEGFA	Vascular Endothelial Growth Factor A
VICs	Valvular Interstitial Cells
VMF	Vascular Mesenchymal Factor

1.Introduction

1.1 Background on Calcific Aortic Valvular Disease - CAVD

Calcific aortic valve disease (CAVD) causes aortic stenosis, affects 25% of people over the age of 65.1 years, and is the most common indication for invasive and expensive valve replacement surgery (Schlotter et al., 2018). Overall, 25% of elderly adults experience thickening of the aortic valves (Carabello & Paulus, 2009; Lindman et al., 2016). The main pathological manifestation in the early stage is aortic valve sclerosis, which gradually develops into aortic valve stenosis (AVS) (Chen et al., 2017). Until recently, the pathogenesis of CAVD was considered a passive degenerative process in the aging process. Nonetheless, current studies have found that it is an active and controllable cell-mediated process, highly like bone development and bone metabolism (Caira et al., 2006). Despite advancements in drug development, and surgery, the disease cannot be cured, and mortality rates remain high. To this day, the only treatment for AVS is aortic valve replacement (Larsson et al., 2017). Thus, a comprehensive understanding of the molecular mechanisms driving CAVD, and the identification of novel therapeutic interventions are crucial for reducing the mortality rate associated with CAVD (Neph et al., 2012).

CAVD is a chronic condition affecting the aortic valve, which is characterized by fibrosis and calcification of the aortic valve tissue (Thompson & Towler, 2012). This may lead to improper valve function, that can cause the development of AVS. AVS stands as the prevailing valvular pathology among the elderly population. Its incidence escalates with age, with a prevalence surpassing 3% in individuals aged 75 years and older (Mathieu, Boulanger, & Bouchareb, 2014). The pathogenesis of CAVD involves distinct changes in the microenvironment of the aortic valve tissue and includes the differentiation of the main cell types inside the valves, called valvular endothelial cells (VECs) and valvular interstitial cells (VICs). VECs form the outer barrier of the tissue and VICs are located inside the tissue (MacGrogan, Münch, & de la Pompa, 2018).

The structure of the human aortic valve is trilaminar, consisting of the fibrosa, spongiosa, and ventricularis layers, which collectively impart the necessary biomechanical properties

to withstand prolonged and repetitive cyclical strains. The fibrosa, facing the aorta, and the ventricularis, facing the ventricle, are primarily composed of collagen and elastic fibers ((Chester et al., 2014)). The arrangement of circumferential collagen in the fibrosa and radial elastic fibers in the ventricularis provides tensile strength and elasticity to the valve cusps during diastole, ensuring optimal coaptation and preventing regurgitation (Sohmer et al., 2018). The spongiosa layer, rich in glycosaminoglycans, forms a loose connective tissue that contributes to the elasticity and compressibility of the valve tissue (Sacks et al., 2009). During embryonic development, the endocardial-to-mesenchymal transition plays a critical role in forming VICs (Monaghan et al., 2016). These cells, comprising a heterogeneous mix of fibroblasts and smooth muscle cells, are essential for maintaining the extracellular matrix and are pivotal in CAVD development. Typically, smooth muscle cells are situated at the base of the ventricular layer in healthy valves, but in CAVD, they cluster around calcified areas (Latif et al., 2015). Aortic valve endothelial cells (VECs), which interact directly with blood flow, are highly responsive to mechanical forces and changes in circulating factors. Unlike vascular endothelium, VECs encounter more complex blood flow patterns and, on the ventricular side of the valve, align perpendicularly to the flow (Deck, 1986). This alignment influences the gene expression profiles in VECs, with those on the aortic surface exhibiting fewer anti-mineralization genes and more prone to pro-inflammatory responses (Lee et al., 2018).

The progression of CAVD is closely associated with specific changes within the aortic valve's microenvironment, particularly concerning the roles of VICs and VECs. These cells are pivotal in the pathology of the disease, where VECs, lining the valve facing the blood flow, respond dynamically to mechanical stresses and biochemical signals (Fernández Esmerats, Heath, & Jo, 2016). VICs, residing within the valve structure, transform under pathological conditions to adopt osteoblastic phenotypes that contribute to valve calcification (Xu et al., 2020). Understanding the cellular behaviors of VECs and VICs in the context of CAVD is crucial for uncovering new therapeutic targets and improving disease management strategies.

VECs become dysfunctional owing to the oscillatory shear stress from irregular blood flow (Chung et al., 2015). This dysfunction results in the secretion of adhesion molecules followed by the adherence of immune cells, such as monocytes and leukocytes, to

endothelial cells (Boström et al., 2011). Subsequently, the secretion of inflammatory cytokines promotes the transmigration of immune cells into the subendothelial space. Within the subendothelial environment, immune cells, particularly monocytes, are activated and later differentiate into macrophages (Towler, 2013). The differentiation leads to the secretion of cytokines and growth factors including tumor necrosis factor (TNF), interleukin-1-β (IL1β), and receptor activator of nuclear factor κB ligand (RANKL), thereby contributing to the osteogenic transition and calcification of VICs (Romas, 2005). In addition, VECs undergo transdifferentiation, which is an endothelial-to-mesenchymal transition (EndMT) (Ma et al., 2020). During this process, endothelial cells acquire mesenchymal cell characteristics and an increased migratory capacity, enabling their transmigration into the subendothelial space (Byon et al., 2008). VEC-derived VICs transition to an osteogenic phenotype (Wang et al., 2017).

Signaling pathways that play a crucial role in the osteogenic transition of VICs are activated during the propagation phase of CAVD; which is a key feature of disease progression. Osteoblastic differentiation in VICs is less dependent on immune cell signaling (Liu et al., 2016). At the molecular level, the differentiation is characterized by the upregulation of calcification markers, including RUNX family transcription factor 2 (RUNX2), alkaline phosphatase (ALPL), bone morphogenic protein 2 (BMP2), and osteocalcin (Hadji et al., 2016). Some important molecules and signalling pathways such as the Notch, BMP2/Smad4 and Wnt signalling pathway, and transcription factor Runx2, that regulate the transdifferentiation of valve mesenchymal cells into osteoblast-like cells have been gradually recognized (Hosen et al., 2022). They are significant in the development of calcified aortic valve disease.

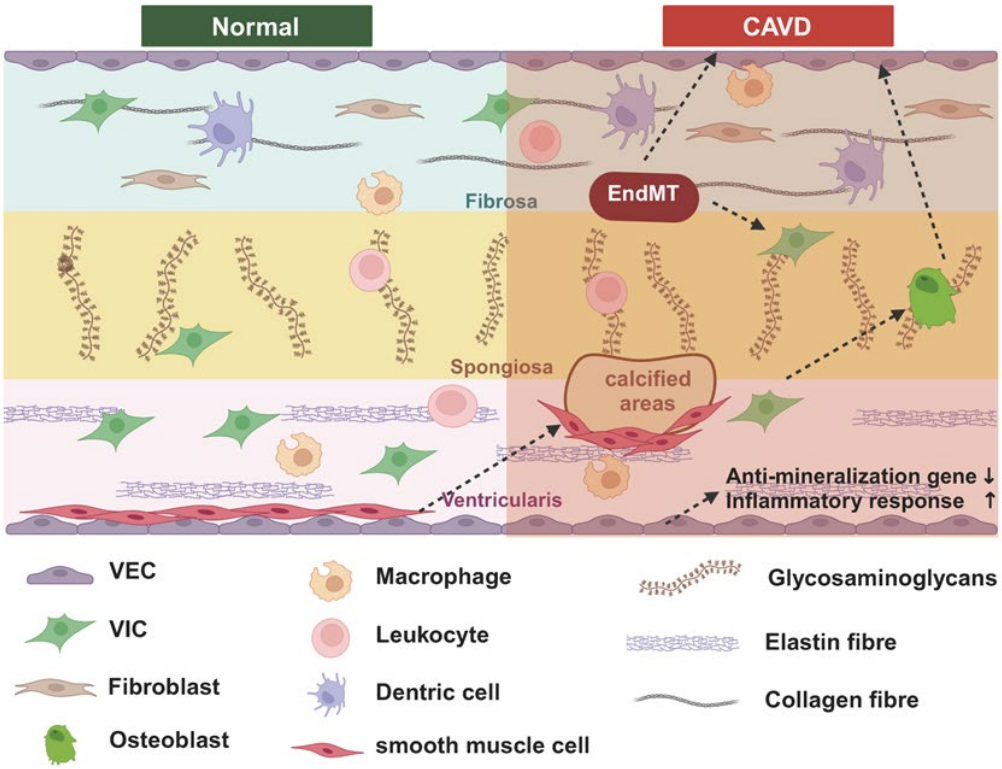

Figure 1. Structural organization of aortic valve: The figure illustrates the differences between normal and CAVD conditions. In normal valves (left side), various cell types such as VECs, VICs, fibroblasts, macrophages, leukocytes, and dendritic cells maintain tissue homeostasis within the three layers of the aortic valve: the fibrosa, spongiosa, and ventricularis. Key structural components like glycosaminoglycans, elastin fibers, and collagen fibers support the valve's architecture. In CAVD (right side), calcified areas appear, and there is an increase in processes like EndMT and inflammatory responses, alongside the upregulation of anti-mineralization genes. VICs transition into osteoblast-like cells, promoting calcification, while smooth muscle cells, inflammatory cells, and macrophages contribute to the progression of CAVD. This figure was created using BioRender.

1.2 Role of Long Non-Coding RNAs in Cardiovascular Diseases

In 2001 the Human Genome Project discovered that approximately 98% of the human genome encodes for ncRNAs (Huang et al., 2020). NcRNAs can be classified according to their length and function into microRNA (miR), long noncoding RNA (LncRNA), circular RNA (circRNA), and other RNA molecules (Engreitz et al., 2016). Recent evidence suggests that ncRNAs play a vital role in aortic valve physiology and pathophysiology (Hosen et al., 2020). MiRs are short RNA molecules with lengths between 19 to 24

nucleotides and function as posttranscriptional regulators by binding messenger RNA (mRNA). miRs are important for cardiovascular development but also play a regulatory role in several cardiovascular diseases. For instance, the differential expression of miRs is associated with cardiovascular diseases such as coronary artery disease, ischemia, and hypertension (Jansen et al., 2016).

LncRNAs are RNA molecules exceeding 200 nucleotides. LncRNAs play crucial roles in transcriptional activation, chromatin modification, X chromosome silencing, and intranuclear transport (Fu, 2014). Moreover, lncRNAs regulate important biological processes, including cell differentiation, proliferation, and apoptosis, thereby contributing to human development (Sallam, Sandhu & Tontonoz, 2018). The relationship between lncRNAs and human diseases gradually became recognized with further research (Garikipati et al., 2019). Recently, it has been discovered that ncRNAs are differentially expressed in CVDs, indicating their potential role in several CVD pathologies, including CAVD (Shen et al., 2017).

LncRNAs are recognized as critical regulators of several cardiovascular diseases (Viereck & Thum, 2017). Nonetheless, knowledge on the contribution of LncRNAs in CAVD and AVS is rather scarce. Thus, it is important to identify novel LncRNA targets and their function in CAVD to elucidate the complex mechanisms of CAVD development and progression.

1.3 Biological Significance of PUNISHER and GAS5

Our recent RNA sequencing analysis between normal and calcified explanted valve tissues from patients with CAVD, which revealed significant dysregulation of lncRNA PUNISHER (also known as AGAP2-AS1) expression. Therefore, we hypothesized that PUNISHER may promotes CAVD progression. Previous studies suggest that PUNISHER plays a critical role in smooth muscle cells and endothelia cells' functions, a key mechanism underlying both atherosclerosis and CAVD (Hosen et al., 2021; Yang et al., 2022). It appears to promote osteogenic differentiation in vascular smooth muscle cells and valvular interstitial cells, contributing to calcium deposition in these tissues. By influencing the expression of essential osteogenic genes, PUNISHER potentially

accelerates the calcification process, underlining its potential as a therapeutic target to prevent or treat calcification-associated cardiovascular conditions.

Since PUNISHER's discovery, lncRNA GAS5 has been extensively investigated for its multifaceted roles in cellular growth, apoptosis, and metabolism, all of which are important in cardiovascular physiology and pathology (Jiang & Ning, 2020). GAS5 acts as a molecular sponge for miRNAs involved in cell cycle regulation and apoptosis (Goustin et al., 2019), thereby exerting a significant effect on the proliferation and survival of cardiovascular cells. In CVDs, the regulatory function of GAS5 in cell proliferation and apoptosis offers insights into its role in atherosclerosis progression (Li et al., 2021). Its ability to influence cellular responses under stress further enforces its importance in CVDs, making it a candidate for biomarker research and therapeutic interventions.

The biological significance of PUNISHER and GAS5 in cardiovascular diseases exemplifies the complex regulatory networks mediated by LncRNAs. Their involvement in key cellular processes relevant to the pathogenesis of CVDs not only advances our understanding of cardiovascular biology but also opens new avenues for the development of LncRNA-based diagnostics and therapeutics. As research continues to unravel the roles of these and other LncRNAs in cardiovascular diseases, targeted strategies to modulate their expression and function hold promise for innovative treatments aimed at improving cardiovascular health.

1.4 Aims of the study

Terefore, the specific aims of this study can be outlined as follows:

1. Dissect the roles of PUNISHER and GAS5 in the calcification process in valvular interstitial cells (VICs) and the EndMT in valvular endothelial cells (VECs)-associated with CAVD.
2. Examine the regulatory effects of PUNISHER and GAS5 on key signaling pathways influencing calcification and the EndMT process in CAVD.

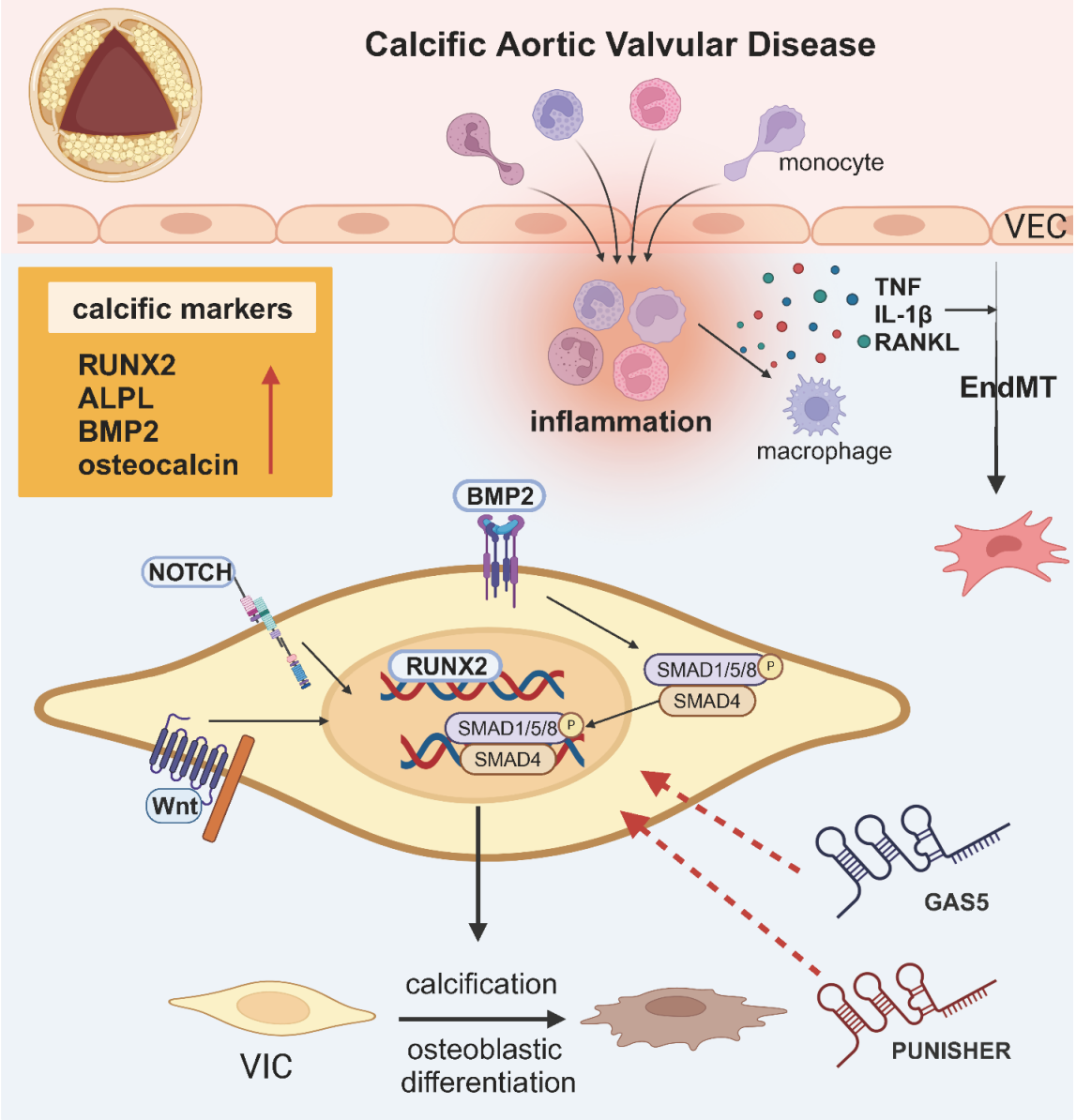

Figure 2. Schematic representation of the pathophysiological mechanisms involved in CAVD. This figure was created using BioRender.

2. Materials and Methods

2.1 Materials

Tab. 1: Information of key resources

Materials	Company	Catalog number
Chemicals and reagents		
Applied Biosystems TaqMan Gene Expression Master Mix	Thermo Fisher Scientific, Waltham, USA (for the first mention)	4369542
Bromodeoxyuridine (BrdU)	BD Biosciences, San Jose, USA	550891
Chloroform	Sigma-Aldrich, St. Louis, USA (for the first mention)	T913.3
DAPI	Vector Laboratories, Newark ,USA	H-1200
Ethanol, ROTIPURAN >99,8%	Carl Roth GmbH Co. G, Karlsruhe, Germany (for the first mention)	4444913
GAS5 siRNA	Thermo Fisher Scientific	4390771
Glycerol-2-phosphate	Sigma-Aldrich	154804-51-0
Hydrochloric acid (HCL)	Carl Roth	9277.1
Hydrogen peroxide solution	SIGMA-Aldrich	H1009
HnRNPK siRNA	Thermo Fisher Scientific	11059
HnRNPU siRNA	Thermo Fisher Scientific	145413

Materials	Company	Catalog number
Interleukin-1β (IL1β)	R&D Systems, Minneapolis, USA (for the first mention)	201-LB-010
L-Ascorbic acid	Sigma-Aldrich	50-81-7
Lipofectamine RNAiMAX	Thermo Fisher Scientific	13778150
Natriumphosphat,NaH2PO4	Sigma-Aldrich	7558-80-7
Paraformaldehyde (PFA)	Sigma-Aldrich	818715
PBS, pH 7,4	Thermo Fisher Scientific	70011051
Pierce IP Lysis Buffer	Thermo Fisher Scientific	87787
Proteinase K	Thermo Fisher Scientific	25530049
PUNISHER siRNA	Thermo Fisher Scientific	4390771
RNase A	Thermo Fisher Scientific	AM2271
Rotiphorese 10x SDS-Page	Carl Roth	3060.2
Silencer Negative Control siRNA	Thermo Fisher Scientific	AM4611
TGFβ	R&D System	240-B-010
TNF-α	R&D Systems	210-TA-020
Triton X-100	Sigma-Aldrich	9002-93-1
TRIzol		
TWEEN 20	SIGMA-Aldrich	P2287
2-Propanol, ROTIPURAN <99,8%	Carl Roth	6752.4
Commercial Kits		
ECL™ Prime Western Blotting Detection Kit	Bio-Rad Laboratories, Hercules, USA (for the first mention)	1705061
High Capacity cDNA Reverse Transcription	Thermo Fisher Scientific	4368813
Human Osteogenesis Taqman Array	Thermo Fisher Scientific	4414096
MTT Cell Growth Assay Kit	MilliporeSigma (a division of Merck KGaA), Burlington, USA	CT02

Materials	Company	Catalog number
Proteome Profiler Human Apoptosis Array	R&D Systems	ARY009
Qubit™ Protein Assay Kit	Thermo Fisher Scientific	Q33211
Cells		
Human Aortic Valve Endothelial Cells (hVEC)	Lonza Group AG, Basel, Switzerland (for the first mention)	00225975
Human Aortic Valve interstitial Cells (hVIC)	Lonza	00225974
Human Coronary Artery Endothelial Cells (HCAEC)	PromoCell GmbH, Heidelberg, Germany (for the first mention)	C-12221
Human Coronary Artery Smooth Muscle Cell (HCASMC)	Promo-cell	C-12512
Mediums		
DMEM, high glucose, GlutaMAX™ supplement	Thermo Fisher Scientific	61965059
Endothelial Cell Growth Medium	Promo-cell	C-22010
Endothelial Cell Growth Medium MV	Promo-cell	C-22020
Fetal Bovine Serum, Qualified, One Shot™ format	Thermo Fisher Scientific	A3160802
Growth Medium MV Supplement Mix	Promo-cell	C-39225
Growth Medium Supplement Mix	Promo-cell	C-39215
Penicillin-Streptomycin (10.000 U/ml)	Thermo Fisher Scientific	15140148
Smooth Muscle Cell Medium(Basis Medium)	Promo-cell	C-22060
Smooth Muscle Cell Medium(Supplement Mix)	Promo-cell	C-22062
Primers		
ACTA2 Hs00426835_g1	Thermo Fisher Scientific	4851370
ALPL Hs01029144_m1	Thermo Fisher Scientific	4331182

Materials	Company	Catalog number
BMP2 Hs00460075_CE	Thermo Fisher Scientific	4351370
GAPDH Hs02758991_g1	Thermo Fisher Scientific	4351368
GAS5 Hs05021116_g1	Thermo Fisher Scientific	4331182
HnRNPK Hs00829140_s1	Thermo Fisher Scientific	4851370
HnRNPU Hs00244919_m1	Thermo Fisher Scientific	4851370
MGP Hs00969490_m1	Thermo Fisher Scientific	4851370
NOS3 Hs01574665_m1	Thermo Fisher Scientific	4851370
PECAM Hs01065279_m1	Thermo Fisher Scientific	4851370
PUNISHER HS01096080_s1	Thermo Fisher Scientific	4426962
RUNX2 Hs01047973_m1	Thermo Fisher Scientific	4851370
TAGLN Hs00162558_m1	Thermo Fisher Scientific	4851370
VEGFA Hs00900054_m1	Thermo Fisher Scientific	4331182
VMF Hs01109446_m1	Thermo Fisher Scientific	4331182
Antibodies		
Anti-ALP antibody	Abcam plc, Cambridge, United Kingdom (for the first mention)	Ab305305
Anti-beta-Actin antibody	Sigma-Aldrich	A1978
Anti-BCL2 Rabbit Polyclonal antibody	Proteintech	12789-1-AP
Anti-Bmp2 antibody	Abcam	Ab214821
Anti-BrdU antibody	Abcam	Ab6326
Anti-CD31 antibody	Abcam	Ab187377
Anti-Mouse IgG	Sigma-Aldrich	A9044-2ML
Anti-MGP antibody	Abcam	Ab273657
Anti-Rabbit IgG	Sigma-Aldrich	A9169-2ML
Anti-RUNX2 antibody	Abcam	Ab23981
Anti-SM22 alpha antibody	Abcam	Ab14106
Anti-VEGFA antibody	Abcam	Ab214424

Materials	Company	Catalog number
Anti-Vimentin antibod	Abcam	ab8978
Donkey Anti-Rabbit-Cy3 IgG antibod	Jackson Immuno Research	712-165-153
MGP Monoclonal Antibody (OTI11G6)	Thermo Fisher Scientific	MA5-26793
Equipment		
Axiovert Microscope 40 CFL	Carl Zeiss AG, Oberkochen, Germany	
ChemiDoc MP Imaging System	Bio-Rad	
CO2 Incubator	Sanyo Denki Co., Ltd., Tokyo, Japan	
NANO DROP 2000c	Thermo Fisher Scientific	
Quant Studio 3 Real-Time PCR System	Thermo Fisher Scientific	-
Quant Studio 5 Real-Time PCR System	Thermo Fisher Scientific	-
Qubit 4 Fluorometer	Invitrogen (part of Thermo Fisher Scientific), Carlsbad, California, USA	
Tecan Infinitie M200 Plate Reader	TECAN, Männedorf, Switzerland	

2.2 Methods

2.2.1 Cell Culture

Human Coronary Artery Endothelial Cells (HCAECs):

HCAECs were cultured in cell growth basal media supplemented with growth media supplement mix (PromoCell, # C-22020, C-22070) under standard conditions (37 °C, 5% CO2). Cells from passages 6–8 were utilized when they reached a confluence of 70–80%.

Smooth Muscle Cells (HCASMCs):

SMCs were maintained in specialized smooth muscle cell media supplemented with the necessary growth factors and serum (Smooth Muscle Cell Medium and Supplement Mix,

#C22060). Standard culture conditions of 37 °C with 5% CO2 were maintained. Cells between passages 5–7, showing 70–80% confluence, were selected for further experiments.

Valve Interstitial Cells (VICs):

VICs (LONZA, #00225974) were propagated in valve interstitial cell-specific media complemented with essential growth supplements (DMEM, high glucose, add 10%FBS and 1% Penicillin-Streptomycin). They were cultured under standard conditions of 37 °C and 5% CO2. For experiments, VICs from passages 5–7 and having a confluence of 70–80% were employed.

2.2.2 Transfection Procedures

Endothelial Cells :

When endothelial cells reached 70% confluence, they were transfected with various siRNAs. The siRNAs used were SCR (serving as a negative control), siPUNISHER, siGAS5, siHNRNPU, and siHNRNPK. The specific product numbers for each siRNA will be provided subsequently. Transfection was executed using 20 nM of the respective siRNA and Lipofectamine RNAiMAX (Thermo Fisher Scientific, #13778150). Cells were then incubated for 48 hours post-transfection, in accordance with the manufacturer's protocol.

Valve Interstitial Cells (VIC) and Smooth Muscle Cells (HCASMCs):

For VIC and HCASMC, transfection was initiated when the cells achieved 60% confluence. The same siRNAs and Lipofectamine RNAiMAX protocol were applied, and post-transfection, cells were allowed to incubate for 48 hours.

2.2.3 In vitro EndMT Induction in HCAECs

HCAECs were cultured in cell growth basal media supplemented with growth media supplement mix under standard conditions (37 °C, 5% CO2). At passage 7 (P7), the cells

underwent transfection. Following transfection, the endothelial-to-mesenchymal transition (EndMT) was induced in HCAECs. For the induction, two different protocols were utilized:
1. Treatment with 30 ng/ml of tumor necrosis factor alpha (TNFα) for 5 days.

2. A combined regimen of 10 ng/ml of transforming growth factor beta 1 (TGFβ1) and 1 ng/ml of interleukin 1 beta (IL1β) for 5 days.

The efficiency and progression of EndMT were subsequently monitored and verified through gene expression analysis using RT-qPCR.

2.2.4 In vitro Calcification Induction in HCASMCs and VICs

For in vitro calcification, two distinct cell types and stimulation protocols were employed:

HCASMCs:

After transfection at passage 8 (P8), HCASMCs were subjected to calcification stimulation. Two distinct media formulations were utilized:

1. Osteogenic Medium (OM): This medium contained 10 nmol/l dexamethasone, 10 mmol/l glycerol-2-phosphate, and 50 µg/ml L-Ascorbic acid.

2. Pro-calcifying medium (PCM): Supplemented with 50 µg/ml L-Ascorbic acid and 2 mmol/l NaH_2PO_4.

Valve Interstitial Cells (VICs):

After transfection at passage 7 (P7), VICs were also exposed to the calcification induction according to our published protocol (Nehl et. al. 2023, Front Card. Medicine).

Both cell types were incubated for 7 days under the respective conditions. Gene expression changes indicating calcification were assessed using quantitative PCR, providing molecular evidence for the process. To visually confirm and quantify mineral deposition, cells were stained with Alizarin Red.

2.2.5 RNA isolation and qRT-PCR

Total RNA from cultured VICs HCASMCs and HCAECs was extracted and isolated using the TRIzol reagent (Thermo Fisher Scientific, #15596018) following the manufacturer's instructions. The concentration of the extracted RNA was quantified using a Nanodrop spectrophotometer. The isolated RNA was then reverse transcribed into cDNA using the High-Capacity cDNA Reverse Transcription Kit (Thermo Fisher Scientific, #43-688-13), adhering to the manufacturer's protocol. Subsequent real-time quantitative PCR analyses for LncRNAs and mRNAs were conducted using the QuantStudio 3/5 Real-Time PCR System from Thermo Fisher Scientific (Waltham, MA, USA). Specific TaqMan® gene expression assays (Applied Biosystems) were utilized in the analysis, with primers in materials table. All samples were run in triplicate. The expression values are presented as 2−[CT(mRNA)-CT(control)] log10.

2.2.6 MTT Assay on VICs

Post-transfection, VICs were seeded in a 96-well plate at 8000 cells/well. For cellular stress induction, cells were treated with 100 μM H_2O_2 and incubated at 37°C with 5% CO_2 for 24 hours. After this period, 0.01 ml of AB Solution from the MTT Cell Growth Assay Kit (Sigma-Aldrich, #CT02) was added to each well and incubated for another 4 hours at 37°C. To dissolve the formazan crystals formed, 0.1 ml of isopropanol mixed with 0.04 N HCl was added. Absorbance was measured using an ELISA plate reader(TECAN, Infinite M200 Microplate reader) at 570 nm, with a reference wavelength of 630 nm.

2.2.7 Proliferation Assessment via BRDU Incorporation

VICs with knocked-down PUNISHER and GAS5 genes were treated and subsequently incubated with BrdU (10 μM, BD) for 24 hours. Following this, cells underwent a membrane permeabilization step and were fixed using 4% PFA. Post-fixation, an acid treatment with hydrochloric acid (HCl) was done to denature the DNA, facilitating BrdU detection. Incorporated BrdU was detected using an anti-rat primary antibody (Abcam,

#ab6326) and visualized with an anti-rat-cy3 secondary antibody (ABCAM, #AB98416). For nuclear staining, a drop of 4’,6-diamidino-2-phenylindole (DAPI, Vector Laboratories, #H-1200) was added to each well. Cell proliferation was analyzed using a Zeiss Axiovert 200M microscope and the captured images were subsequently processed with ImageJ.

2.2.8 Immunofluorescence Staining

HCASMCs were fixed with 4% formaldehyde for 30 min in 24-well plates with glass coverslips. After rinsing three times with 1× PBS, cells were permeabilized using 0.25% Triton X-100 in PBS for 10 min, followed by three additional washes with 1× PBS. Blocking was done using 1% BSA-glycine in PBS with 0.1% Tween for 30 min. The cells were then incubated with the primary antibody BMP2 (Abcam, #AB214821) for overnight on a shaker.

After primary antibody incubation, cells were washed three times with 1× PBS. Subsequently, they were incubated with an anti-rabbit-cy3 secondary antibody (Dianova, #111-165-144) on a shaker for 1 h. Following the secondary antibody application, cells underwent three more washes with 1× PBS and were then mounted using Vectashield® Antifade Mounting Medium with DAPI (Vectashield, #H-1200-10). The staining was visualized using a Zeiss Axiovert 200M microscope.

2.2.9 Western Blot

Total protein was extracted from cultured cells using the ice-cold Pierce IP Lysis Buffer (Thermo Scientific, #87787), supplemented with a protein inhibitor cocktail (Roche, #11 873 580 001) at 4°C. Protein concentrations were ascertained using the Qubit Protein Assay Kit (Thermo Fisher Scientific, #Q33211) on the Qubit 4.0 Fluorometer (Thermo Fisher Scientific). Equal amounts of each protein sample were subjected to 4–15% Mini-Protean gels (Bio-Rad, #4565014). After electrophoresis, proteins were transferred onto NC membranes (Carl Roth, Transfer membrane ROTI®NC 0.2, Ø 9.0 cm). Membranes were then blocked with a 5% BSA-TBST solution for one hour at room temperature with

gentle agitation. For primary antibody incubation, membranes were exposed overnight at 4°C to the following antibodies:

Antibody	**Company and Catalog number**	**Concentration**
Anti-ß-Actin (internal reference)	Sigma-Aldrich, A1978	1:1000
Anti-RUNX2	Abcam, Ab23981	1:1000
Anti-BMP2	Abcam, Ab214821	1:1000
Anti-BCL-2	Proteintech, 12789-1-AP	1:1000
Anti-MGP	Abcam, Ab273657	1:1000
Anti-VEGFA	Abcam, Ab214424	1:1000
Anti-CD31	Abcam, Ab187377	1:1000
Anti-Vimentin	Abcam, Ab8978	1:1000
Anti-SM22	Abcam, Ab14106	1:1000

Following primary antibody binding, membranes were treated with the appropriate secondary antibodies either mouse or rabbit, depending on the primary antibody source (Anti-Mouse IgG, Sigma-Aldrich, A9044-2ML, Anti-Rabbit IgG, Sigma-Aldrich, A9169-2ML). Visualization was done using the Clarity Western ECL Substrate (Bio-Rad, #1705061), and images were captured on a ChemiDoc MP Imaging System (Bio-Rad). The band intensities were quantified using ImageJ, with normalization to ß-Actin serving as the internal control.

2.2.10 Apoptosis Protein Array Analysis of Calcification-induced Transfected VICs

Following transfection and a subsequent 7-day calcification induction as described in section 2.2.4, proteins were extracted from the treated VICs. The extraction procedure mirrored the protocol utilized for Western blotting. Specifically, cells were lysed using the ice IP Lysis Buffer (Thermo Scientific, #87787), enriched with a protein inhibitor cocktail (Roche, #11 873 580 001) at 4°C. Protein concentrations were then determined using the Qubit Protein Assay Kit (Thermo Fisher Scientific, #Q33211) on the Qubit 4.0 Fluorometer (Thermo Fisher Scientific). For the subsequent protein profiling, the Proteome Profiler Array, specifically the Human Apoptosis Array Kit (R&D Systems, #ARY009, Minneapolis, MN, USA), was employed. Each array was loaded with 200 µg of protein to ensure comprehensive analysis. Adhering to the manufacturer's instructions, the array was processed to detect potential protein interactions or modifications. The data generated from these arrays were meticulously analyzed to pinpoint significant patterns or shifts in protein expression or activity, which could be attributed to the calcification process in the transfected VICs.

2.2.11 TaqMan Array Human Osteogenesis Analysis of Calcification-induced Transfected VICs

After the transfection and the 7-day period of calcification induction outlined in section 2.2.4, we proceeded to assess the expression levels of osteogenesis-related genes in the treated VICs. The RNA was isolated using a standard extraction protocol. The quantified RNA was then reverse-transcribed to cDNA, which was used as a template for the TaqMan Array Human Osteogenesis. This high-throughput quantitative PCR (qPCR) platform (Thermo Scientific, # 4414096) allowed for the simultaneous analysis of a panel of genes associated with osteogenic differentiation and bone formation. Each well of the array contained pre-dispensed TaqMan Gene Expression Assays, designed to amplify gene-specific regions of interest.

The qPCR was performed on a QuantStudio 3 Flex Real-Time PCR System, following the manufacturer's protocol. This enabled the amplification and detection of target gene

expression levels, which were later analyzed for relative quantification against housekeeping genes, using the ΔΔCT method. Data from this comprehensive gene expression profiling provided insights into the osteogenic potential and the differentiation status of VICs in response to the calcification conditions and gene knockdown interventions.

2.2.12 Statistical Analysis

Normally distributed continuous variables were presented as the mean ± SD. Continuous variables were tested for a normal distribution with the use of the Kolmogorov–Smirnov test. Categorical variables were presented as frequencies and percentages. For continuous variables, Student t-test or Mann–Whitney U was used for comparison between two groups. For the comparison of >2 groups, the repeated measures ANOVA with Bonferroni's correction for multiple comparisons test was used. A Chi-square test was used for the categorical data. All tests were 2-sided and statistical significance was assumed when the null hypothesis could be rejected at $p < 0.05$. Statistical analysis was performed with IBM SPSS Statistics version 24 (USA) and GraphPad Prism 9.

3. Results

3.1 Impact of lncRNAs Dysregulation on Endothelial-to-Mesenchymal Transition (EndMT) in HCAECs

3.1.1 PUNISHER Expression changes in HCAECs:

During the EndMT treatment, HCAECs displayed augmented levels of PUNISHER, implying its potential involvement in endothelial transitions (Fig.3A).

3.1.2 GAS5 Expression changes in HCAECs:

Upon induction of EndMT in HCAECs, there was a notable increase in GAS5 levels, indicating its potential role in the process (Fig.3B).

3.1.3 Knockdown of PUNISHER and GAS5 in HCAECs:

Post siRNAs transfection, a significant reduction in the expression levels of PUNISHER and GAS5 was observed. The effective knockdown of PUNISHER and GAS5 in HCAECs was validated through qPCR (Fig. 3C-D). This established a solid foundation for the subsequent functional experiments and protein analysis, aimed at understanding the roles of these genes in CAVD.

3.1.4 RT-qPCR Analysis of EndMT Markers (ACTA2 and VMF):

We analyzed the expression of EndMT markers ACTA2 and VMF in HCAECs using RT-qPCR (Fig.3E-F). Post-EndMT induction with TNFα, there was a noticeable increase in ACTA2 and VMF levels, particularly following the knockdown of lncRNAs PUNISHER and GAS5. This suggests that these lncRNAs may influence the EndMT process by modulating

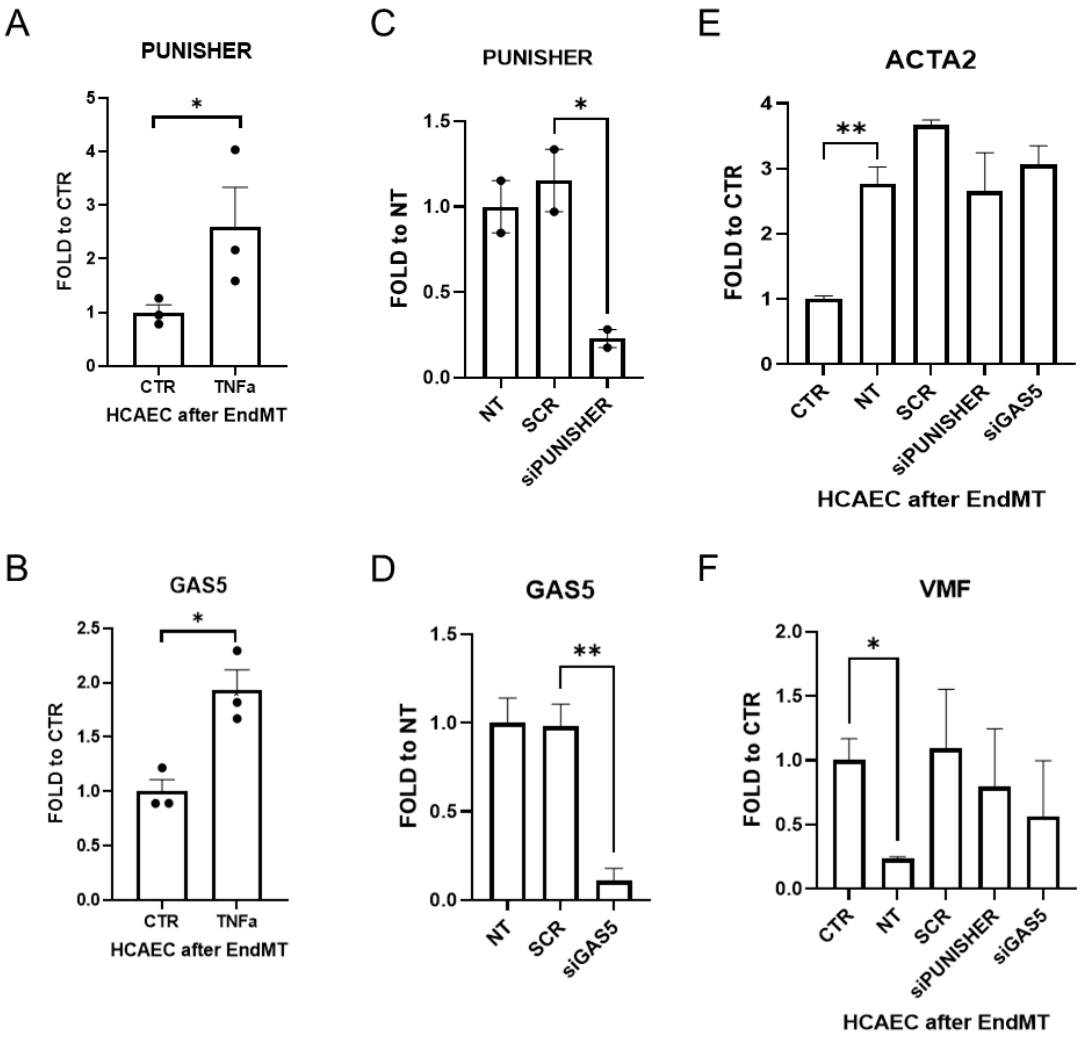

Figure 3. Impact of LncRNAs dysregulation on HCAECs after EndMT and knockdown. Expression levels of PUNISHER (A) and GAS5 (B) in HCAECs post-endothelial-to-mesenchymal transition (EndMT), stimulated by tumor necrosis factor alpha (TNFα), compared to control (CTR). Data are expressed as mean fold change ± SEM from three independent experiments (n=3); *p < 0.05. Knockdown effects on PUNISHER (C) and GAS5 (D) expression in HCAECs. NT (non-treated); SCR (scrambled siRNA control); siPUNISHER and siGAS5, specific siRNAs targeting PUNISHER and GAS5, respectively. Data normalized to NT, represent mean fold change ± SEM from three independent experiments (n=3); *p < 0.05, **p < 0.01. Quantitative PCR analysis of ACTA2 (E) and VMF (F) expression in HCAECs post-EndMT under different treatment conditions. Columns represent mean fold change relative to control ± SEM from three independent experiments (n=3); *p < 0.05, **p < 0.01. The data were analyzed using t-tests for each group.

3.1.5 Morphological Changes in HCAECs Post-EndMT:

In this part of the study, we used a microscope to look at HCAEC cells and saw them change shape due to TNFα treatment (Fig. 4A). They went from looking like paving stones to long and thin shapes.

3.1.6 Cell Migration Assays Post-Knockdown

Scratch assay (Fig.4B) results for HCAECs post PUNISHER and GAS5 knockdown. The panels show representative images at 0, 4, and 8 hours post-scratch for NT, SCR, siPUNISHER, and siGAS5 treated cells. Below, the graph quantifies the percentage of wound healing area over time, highlighting the slower migration in siPUNISHER and siGAS5 groups compared to controls, indicating a role in endothelial cell motility and repair mechanisms.

3.1.7 Western Blot Analysis of EndMT-Related Proteins (CD31, VEGFA, ALPL, Vimentin)

Western blot analysis (Fig. 4D) was conducted to assess the expression levels of CD31, ALPL, Vimentin, and VEGFA in HCAECs subjected to TNFα-induced EndMT following knockdown of PUNISHER and GAS5. β-actin served as a loading control. Post-TNFα stimulation, there was an increase in Vimentin expression, indicative of successful EndMT, while CD31 and VEGFA levels decreased, further confirming the EndMT phenotype. Notably, knockdown of PUNISHER and GAS5 also led to significant changes in the expression of ALPL, VEGFA, and Vimentin, highlighting the potential mechanisms through which these lncRNAs may influence endothelial cell function and the EndMT process.

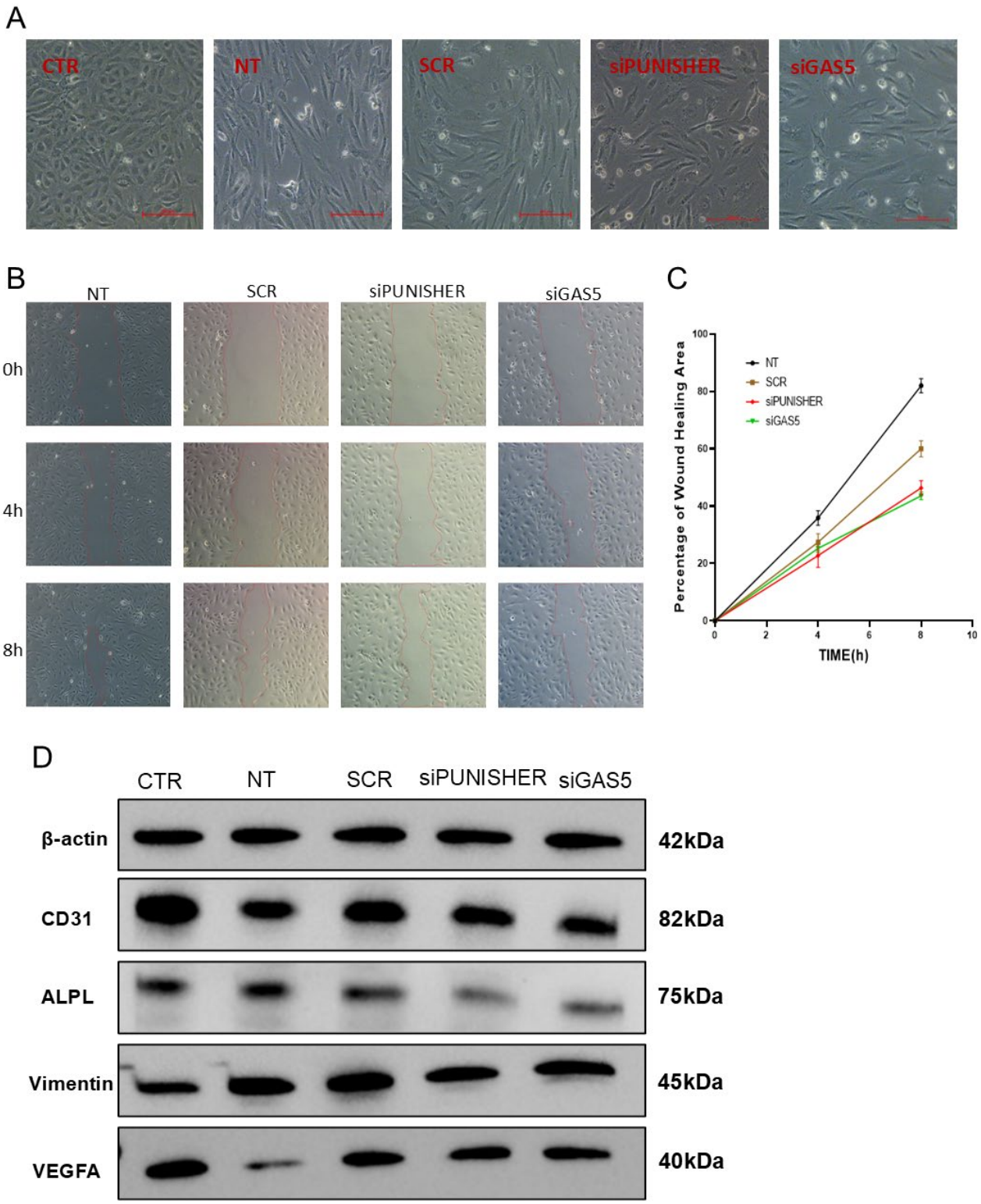

Figure 4. LncRNAs play a role in function and cell properties of EC during EndMT.

(A) Morphological changes in HCAECs after five days of TNFα exposure to induce EndMT. The images show variations in cell morphology across different experimental setups including Control (CTR, untreated), non-transfected (NT), scrambled siRNA control (SCR), siPUNISHER, and siGAS5 treated cells, emphasizing the cellular adaptations to EndMT. (B-C) Scratch assay of HCAEC cell migration post-siRNA treatment. Sequential images depict the migratory response of HCAECs at 0, 4, and 8 hours post-wound infliction under different treatment conditions: NT, SCR, siPUNISHER, and siGAS5. The corresponding graph quantifies the percentage of wound healing area over time. Statistical analysis using t-tests indicates significant reductions in wound healing percentages in the siPUNISHER and siGAS5 groups compared to the SCR group ($p < 0.05$). (D) Western blot analysis of EndMT markers including β-actin (loading control), CD31 (endothelial marker), ALPL (mesenchymal marker), Vimentin (mesenchymal marker), and VEGFA (angiogenesis marker) across different treatment groups. The data illustrate the molecular changes associated with the EndMT process in HCAECs and the impact of specific gene knockdowns on the expression of these key proteins.

3.2 Influence of PUNISHER and GAS5 on Calcification Processes in HCASMCs

3.2.1 Altered Expression of PUNISHER and GAS5 in HCASMCs Under Calcification Stimulation

The expression levels of PUNISHER and GAS5 were significantly altered in HCASMCs following calcification stimulation (Fig5A). Treatment with osteogenic medium (OM) and pericyte culture medium (PCM) increased the expression of both lncRNAs, demonstrating their responsiveness to calcification cues. PUNISHER expression was notably higher in cells treated with OM compared to those treated with PCM, while GAS5 showed a consistent increase under both conditions.

3.2.2 Assessment of Calcification Markers in HCASMCs Post-Knockdown and Calcification Stimulation

Following the knockdown of PUNISHER and GAS5 (Fig.5B), significant changes were observed in the levels of calcification markers in HCASMCs. The expression of ALPL, BMP2, and RUNX2 was assessed under OM and PCM conditions (Fig.5C-D). The data indicate that knockdown of either lncRNA modulates the expression of these markers, suggesting their roles in the regulation of calcification pathways. Notably, the knockdown of PUNISHER resulted in a pronounced decrease in ALPL and BMP2 expression under OM conditions, highlighting its potential role in promoting calcific responses.

3.2.3 Western Blot Analysis of Calcification Markers Post-Knockdown

Western blot analysis (Fig.5E) was performed to further validate the impact of lncRNA knockdown on the protein levels of key calcification markers in HCASMCs. The proteins analyzed included Runx2, MGP, and BMP2. Results showed that the protein levels were affected by the knockdown of PUNISHER and GAS5, corroborating the qPCR findings. Notably, the levels of Runx2 and BMP2 were reduced in cells where PUNISHER and GAS5 were knocked down, indicating the crucial role these lncRNAs play in the regulation of osteogenic differentiation in HCASMCs.

3.2.4 Impact of PUNISHER and GAS5 Knockdown on Cell Migration and Proliferation

In the scratch assay conducted on HCAMSC (Fig.6), we observed the migration patterns post-siRNA treatment targeting PUNISHER and GAS5. The assay monitored cell migration at 0, 4, and 16 hours after a wound was manually created in the cell monolayer. The different treatment groups, NT, SCR, siPUNISHER, siGAS5, showed distinct migration behaviors, which were captured through sequential microscopy images.

These images distinctly illustrate the progressive closure of the wound over time. The corresponding quantitative analysis, depicted in the graph, measures the percentage of wound closure area, highlighting differences in cellular motility among the treatment conditions. This data provides significant in=ights into how genetic modulation of PUNISHER and GAS5 can affect cell dynamics, critical for understanding their potential therapeutic roles in vascular repair and regeneration.

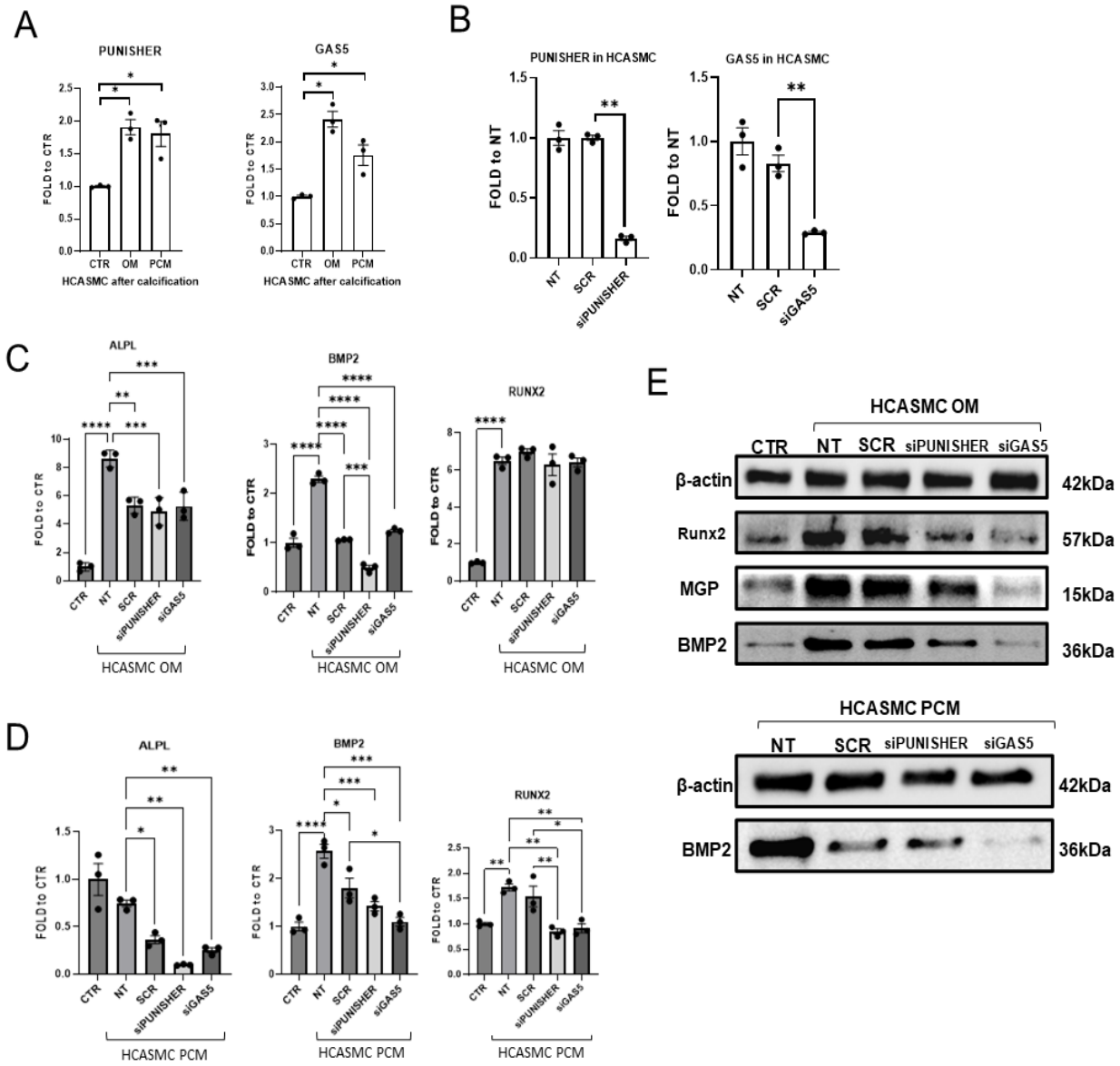

Figure 5: Influence of PUNISHER and GAS5 on calcification in HCASMCs. (A) Expression of PUNISHER and GAS5 in HCASMCs after stimulation with OM or PCM for 7 days, relative to CTR. Data are presented as fold change to CTR (n=3) and analyzed using t-tests (*p < 0.05, **p < 0.01). (B) Knockdown efficiency of PUNISHER and GAS5 in HCASMCs transfected with SCR, siPUNISHER, or siGAS5, shown as fold change relative to non-transfected cells (NT). Statistical analysis was performed using t-tests (**p < 0.01, n=3). (C-D) mRNA expression levels of osteogenic markers ALPL, BMP2, and RUNX2 in HCASMCs cultured in OM (C) or PCM (D), under different conditions: CTR, NT, SCR, siPUNISHER, and siGAS5. Data are normalized to CTR and shown as fold change

(n=3), analyzed using t-tests (*p < 0.05, **p < 0.01, ***p < 0.001, ****p < 0.0001). (E) Western blot analysis showing the protein expression levels of Runx2, MGP, and BMP2 in HCASMCs under OM and PCM conditions post-lncRNA knockdown. The blots reveal differential expression patterns correlating with the knockdown of PUNISHER and GAS5, supporting their functional involvement in calcific pathways.

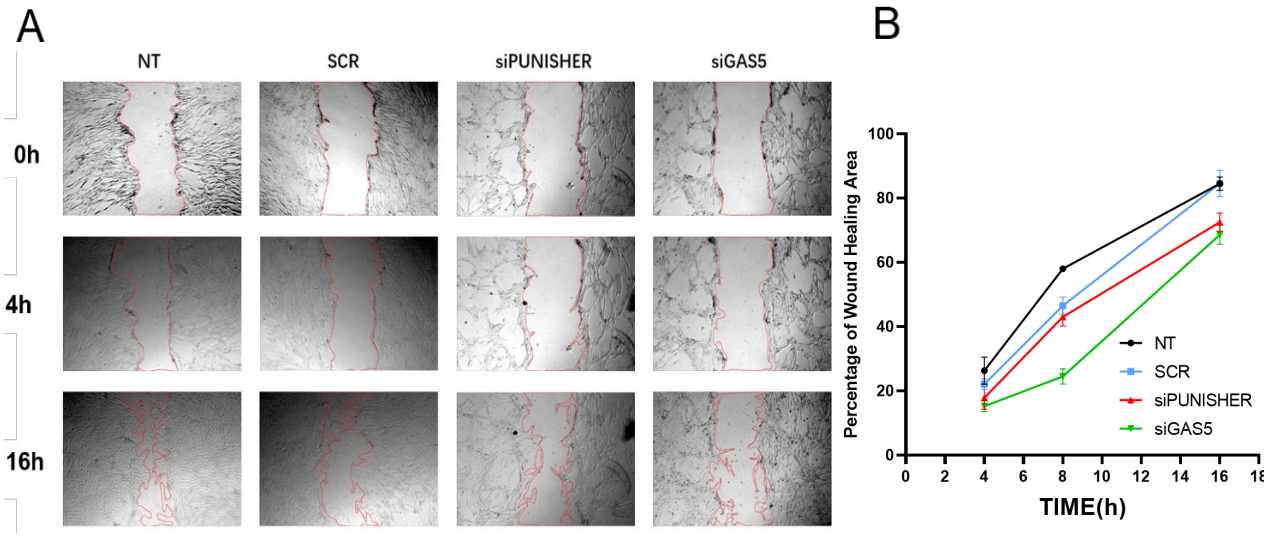

Figure 6: Scratch Assay of HCASMC Cell Migration Post-siRNA Treatment. (A) Sequential images depict the migratory response of HCASMCs at 0, 8, and 16 hours under different conditions: NT, SCR, siPUNISHER, and siGAS5. (B) The corresponding graph quantifies the percentage of wound healing area over time. Statistical analysis using t-tests shows significantly reduced migration at 16 hours in the siPUNISHER and siGAS5 groups compared to SCR ($p < 0.05$), emphasizing the impact of lncRNA knockdown on HCASMC migration.

.

3.3 Role of PUNISHER and GAS5 in VIC Calcification

3.3.1 Expression of PUNISHER and GAS5 in VICs Post-Calcification

Post-calcification, VICs exhibited a significant upregulation in the expression of PUNISHER and GAS5 (Fig.7A). The OM and PCM conditions induced notable increases in both lncRNAs, with PUNISHER showing marked responsiveness to the control condition.

3.3.2 Knockdown of PUNISHER and GAS5 in VICs

The knockdown efficiency of siPUNISHER and siGAS5 in VICs was confirmed by RT-qPCR, showing a significant reduction in mRNA levels compared to NT and SCR controls under both OM and PCM conditions(Fig.7B).

3.3.3 Assessment of Calcification Markers in VICs Post-Knockdown and Calcification Stimulation

Following siRNA-mediated knockdown and calcification stimulation, significant changes were observed in key calcification markers. ALPL and RUNX2 levels increased under OM stimulation, suggesting enhanced osteogenic activity, which was modulated differently by the knockdown of PUNISHER and GAS5 (Fig7. C-D).

3.3.4 Western Blot Analysis of Calcification Markers Post-Knockdown

Protein analysis via Western blot showed changes in MGP and BMP2 levels after knockdown and OM treatment, reflecting the molecular impacts of LncRNA modulation on calcification pathways in VICs (Fig.7 E).

3.3.5 MTT Assay on VICs Post-Treatment

The MTT assay indicated that VIC viability was significantly influenced by the knockdown of PUNISHER and GAS5 (Fig7. F), with observable differences in cell viability between treated and control groups, emphasizing the potential regulatory role of these LncRNAs in cell survival.

3.3.6 Proliferation Assessment via BRDU Incorporation

The BrdU staining results for VICs post-transfection indicate a significant decline in cell proliferation rates upon knockdown of LncRNAs PUNISHER and GAS5. Notably, non-transfected (NT) cells and those treated with scrambled RNA (SCR) maintained higher BrdU incorporation rates, suggesting that the observed reductions in proliferation are specifically related to the silencing of these LncRNAs. This outcome aligns with

expectations and underscores the potential regulatory influence of PUNISHER and GAS5 on cell proliferation.

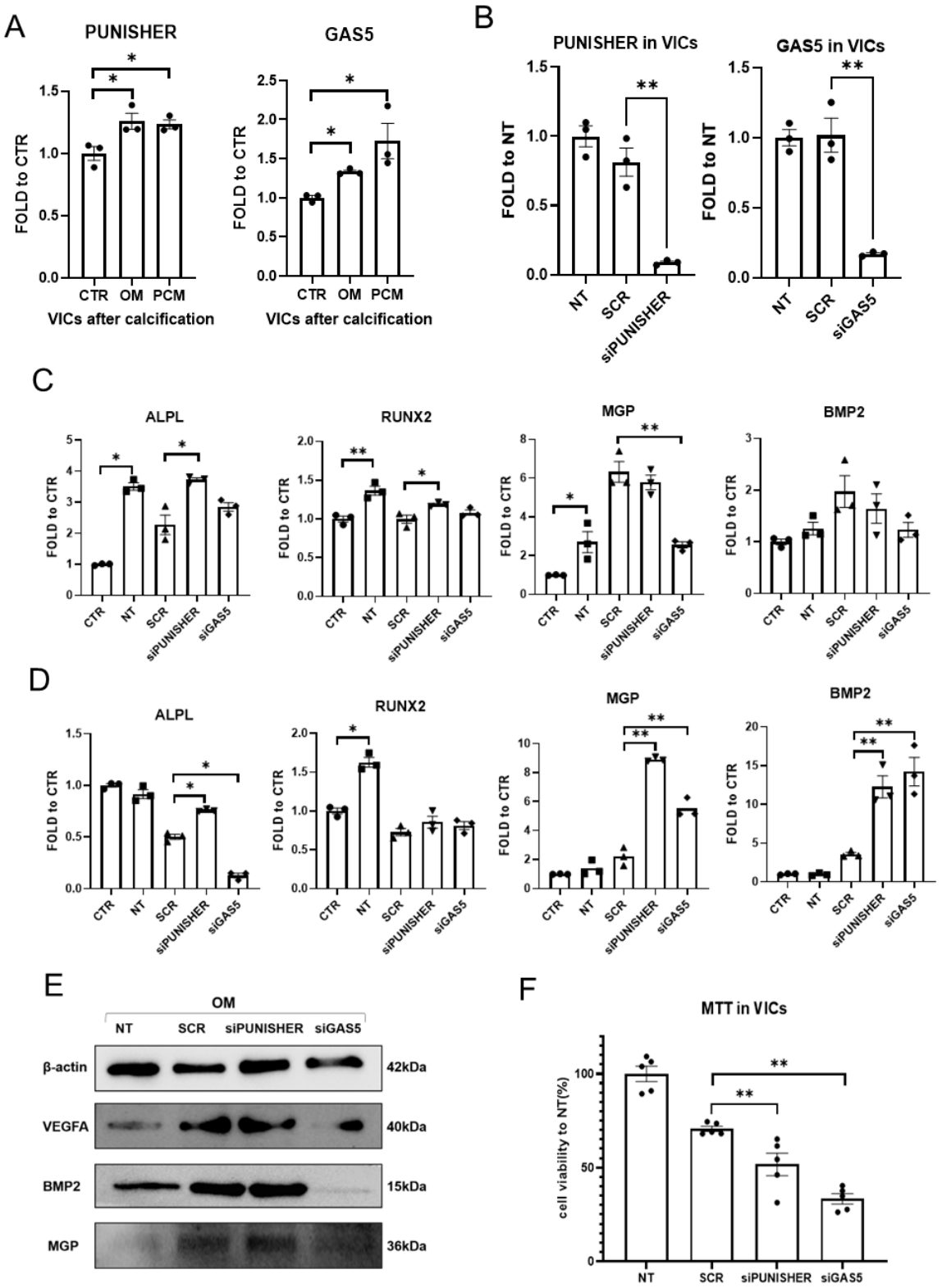

Figure 7. (A) RT-qPCR analysis of PUNISHER and GAS5 expression in VICs after treatment with OM or PCM. Both lncRNAs are significantly upregulated post-calcification treatment (*p < 0.05, n=3, t-tests). (B) siRNA-mediated knockdown efficiency of PUNISHER and GAS5 in VICs, showing a significant reduction in their expression levels compared to NT and SCR controls (**p < 0.01, n=3, t-tests). (C) mRNA expression levels of calcification markers ALPL, RUNX2, BMP2, and MGP in VICs following PUNISHER and GAS5 knockdown under OM conditions (*p < 0.05, **p < 0.01, n=3, t-tests). (D) mRNA expression levels of the same calcification markers in VICs following knockdown under PCM conditions (*p < 0.05, **p < 0.01, n=3, t-tests). (E) Western blot images depicting the protein levels of BMP2, MGP, and VEGFA in VICs post-siRNA treatment under OM condition, providing insights into the protein dynamics associated with LncRNAs modulation. (F) MTT assay results showing the effects of PUNISHER and GAS5 knockdown on VIC viability, highlighting significant reductions in cell survival and proliferation compared to NT and SCR controls (*p < 0.05, **p < 0.01, n=3, t-tests).

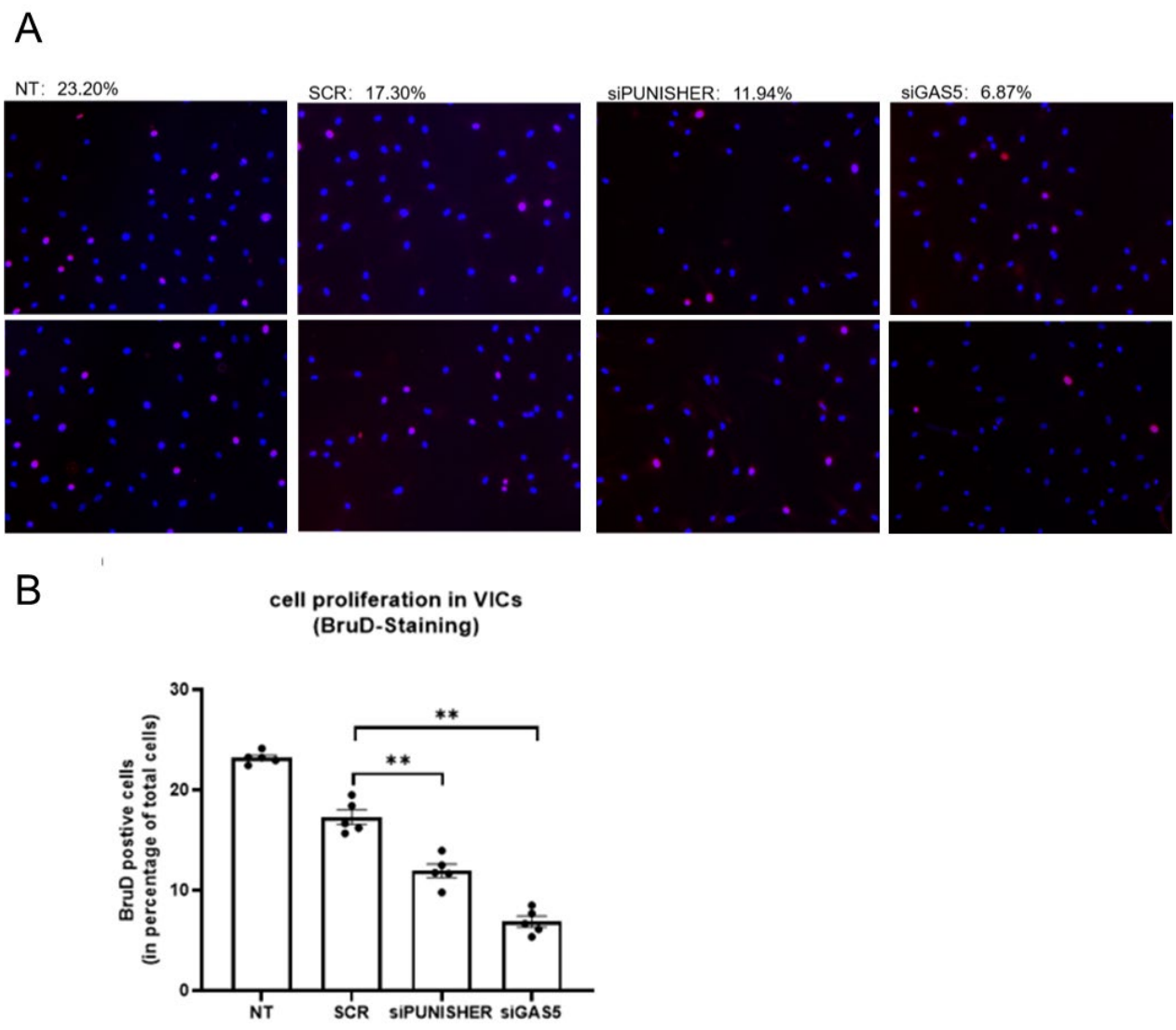

Figure 8. PUNISHER and GAS5 in valve interstitial cell proliferation.

BrdU incorporation assay results demonstrating cell proliferation rates under the same conditions, with a marked reduction in proliferation upon siPUNISHER and siGAS5 treatment. (A) Representative fluorescence microscopy images from the BrdU assay show DAPI-stained nuclei in blue and BrdU-positive cells in red, indicating proliferating cells. (B) The reduction in red signal correlates with the decrease in cell proliferation observed in siRNA-treated groups. **$p < 0.01$ signifies statistical significance between groups.

3.4 Molecular Effects of LncRNA Modulation in VICs

3.4.1 Differential Gene Expression Post-LncRNA Knockdown and Calcification Treatment

In the comprehensive analysis of gene expression modifications following the knockdown of LncRNAs PUNISHER and GAS5, we deployed a TaqMan Array Human Osteogenesis Analysis to visualize the regulatory impacts on gene expression within VICS. The data was visualized through volcanic plots which clearly illustrated significant changes in gene expression. For PUNISHER knockdown, key osteogenic markers like ALPL and VEGFB were significantly upregulated, suggesting enhanced osteogenic activity. Conversely, critical regulatory genes such as TGFBR1 and COL15A1 showed notable downregulation, indicating a suppression of pathways inhibiting calcification. Similarly, GAS5 knockdown resulted in the upregulation of BMP2 and COL4A4, while downregulating TGFB3 and IGF1R, highlighting its role in modulating growth factor-related pathways.

A

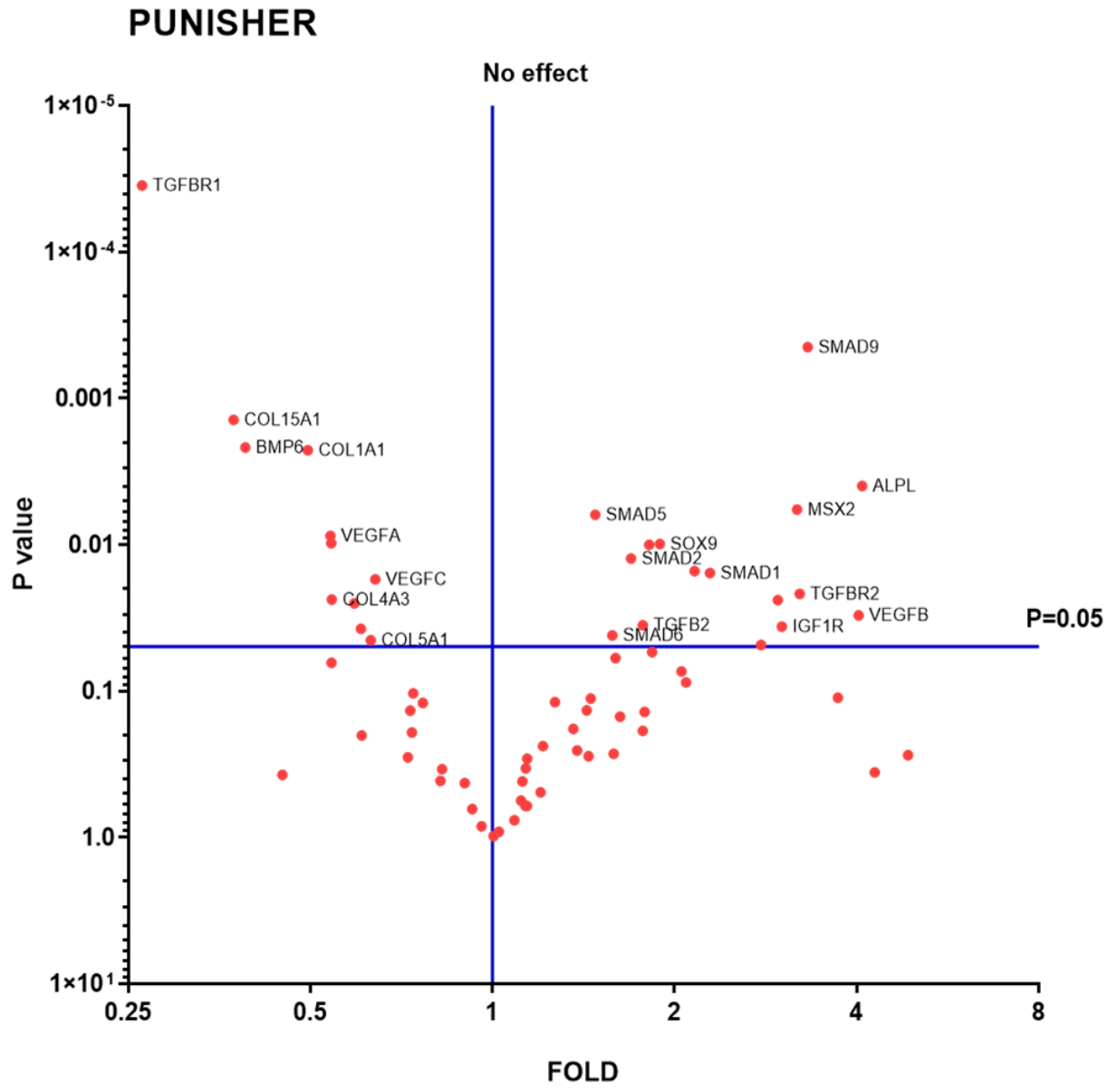

Top 5 Dysregulated Gene in Target VICs (Post PUNISHER Knockdown)					
Downregulated	Fold Change	P Value	Upregulated	Fold Change	P Value
TGFBR1	0.263	0.0001	ALPL	4.087	0.0039
COL15A1	0.373	0.0014	VEGFB	4.031	0.030
BMP2	0.390	0.0022	SMAD9	3.319	0.0004
COL1A1	0.495	0.002	TGFBR2	3.221	0.217
VEGFA	0.540	0.008	MSX2	3.189	0.006

B

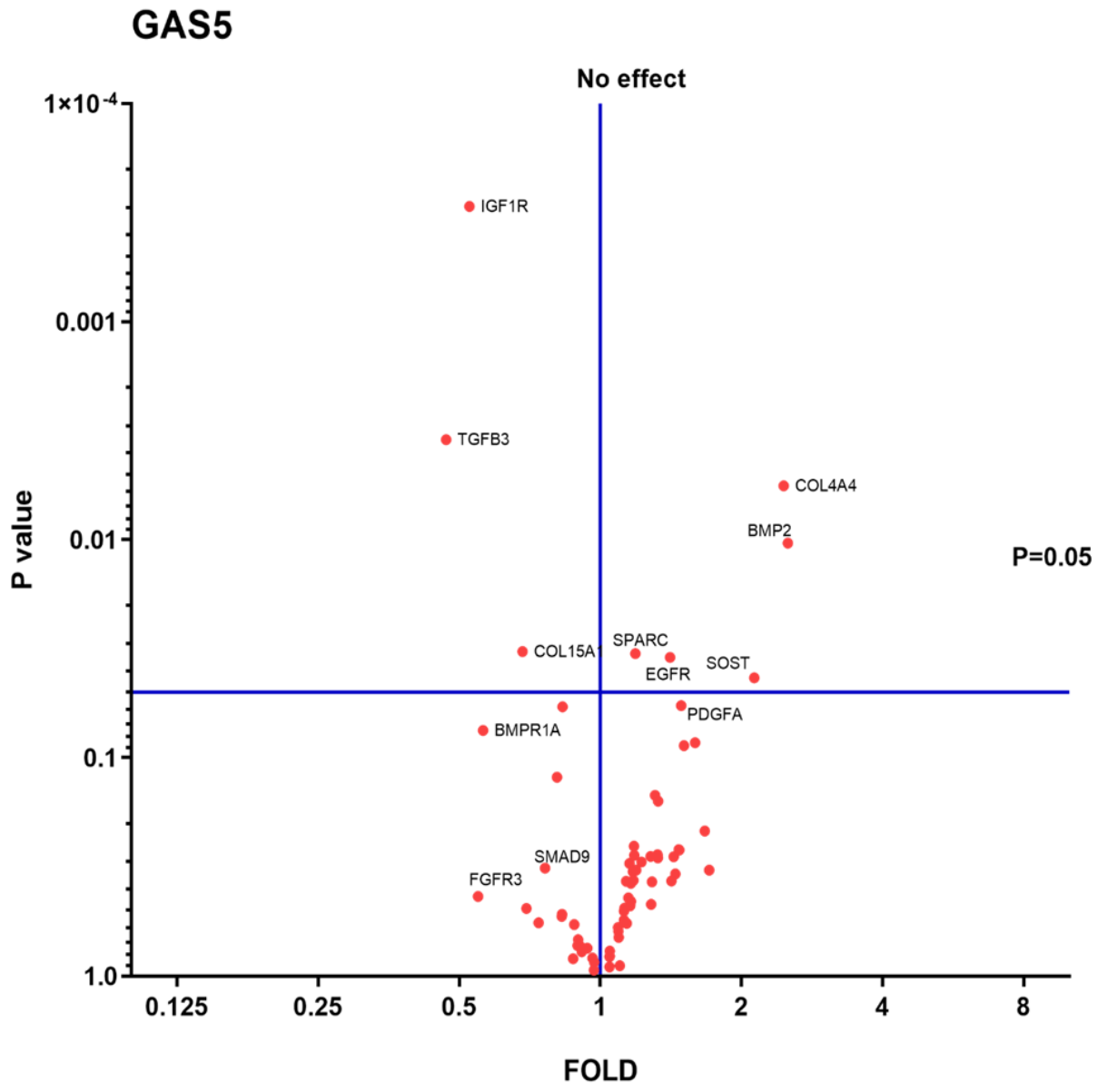

Top 5 Dysregulated Gene in Target VICs (Post GAS5 Knockdown)					
Downregulated	Fold Change	P Value	Upregulated	Fold Change	P Value
TGFB3	0.469	0.003	BMP2	2.513	0.010
IGF1R	0.525	0.0002	COL4A4	2.461	0.0056
FGFR3	0.549	0.432	SOST	2.131	0.043
BMPR1A	0.563	0.748	EGFR	1.409	0.034
COL15A1	0.682	0.0325	SPARC	1.187	0.033

Figure 9. Differential Gene Expression in VICs Post-Knockdown and calcification treatment of PUNISHER and GAS5. The volcano plots illustrate the differential gene expression in VICs following the knockdown of PUNISHER (A) and GAS5 (B). Significant gene expression changes are highlighted, with upregulated genes shown above and downregulated genes below the P=0.05 significance threshold line. Data are based on n=3 biological replicates and analyzed using t-tests for statistical significance.

3.4.2 Apoptotic Response to LncRNA Knockdown in VICs

The Proteome Profiler Array results illustrate pronounced alterations in protein expression linked to both intrinsic and extrinsic apoptotic pathways, accentuating the profound biological impact of knockdown experiments with various genes. Specifically, the differential expression patterns observed across the samples—ranging from non-treated (NT) controls to targeted gene silencing using siRNA against PUNISHER, GAS5, HNRNPU, and HNRNPK—highlight how each gene's modulation distinctly influences the apoptotic signaling within valvular interstitial cells (VICs). These changes are especially evident in the variation of key apoptotic markers such as caspases, Bcl-2 family proteins, and SMAC/DIABLO, offering valuable insights into their potential mechanistic roles in VIC pathophysiology related to calcific aortic valve disease.

A

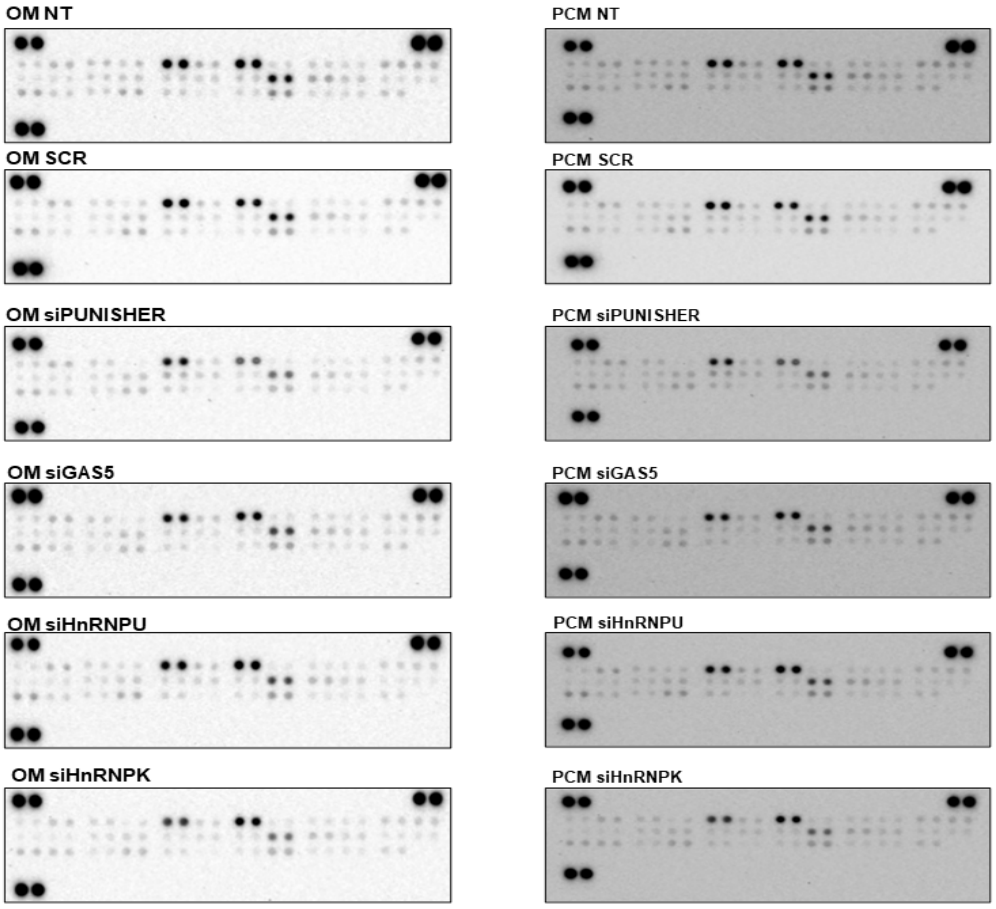

B

	1	2	3	4	5	6	7	8	9	10	11	12	13	14	15	16	17	18	19	20	21	22	23	24
A	Reference spots																						Reference spots	
B	Bad		Bax		Bcl-2		Bcl-x		Pro-caspase-3		Cleaved caspase-3		Catalase		cIAP-1		cIAP-2		Claspin		Clusterin		Cytochrome C	
C	TRAIL R1/DR4		TRAIL R2/DR5		FADD		Fas/TNFRSF6/CD95		HIF-1α		HO-1/ HMOX1		HO-2/ HMOX2		HSP27		HSP60		HSP70		HTRA/Omi		Livin	
D	PON2		p21/CIP1/ CDKN1A		p27/Kip		Phospho-p53 (S15)		Phospho-p53 (s46)		Phospho-p53 (S392)		Phospho-Rad17 (S635)		SMAC/ Diablo		Survivin		TNF RI/ TRFRSF1A		XIAP		PBS	
E	Reference spots																							

Figure 10: (A) Proteome Profiler of apoptotic pathways activation in VICs post LncRNAs knockdown. This array showcases the shifts in protein expression related to apoptotic pathways in VICs following knockdown of specific lncRNAs and other genes. Each panel represents a different treatment condition: non-treated (NT), scrambled siRNA (SCR), and specific knockdowns (siPUNISHER, siGAS5, siHNRNPU, siHNRNPK) under OM and PCM stimulation. (B)Key apoptotic proteins, including caspases, Bcl-2 family proteins, and apoptotic regulators, are mapped, illustrating the cellular response to gene silencing in two different calcific environments.

OM part 1

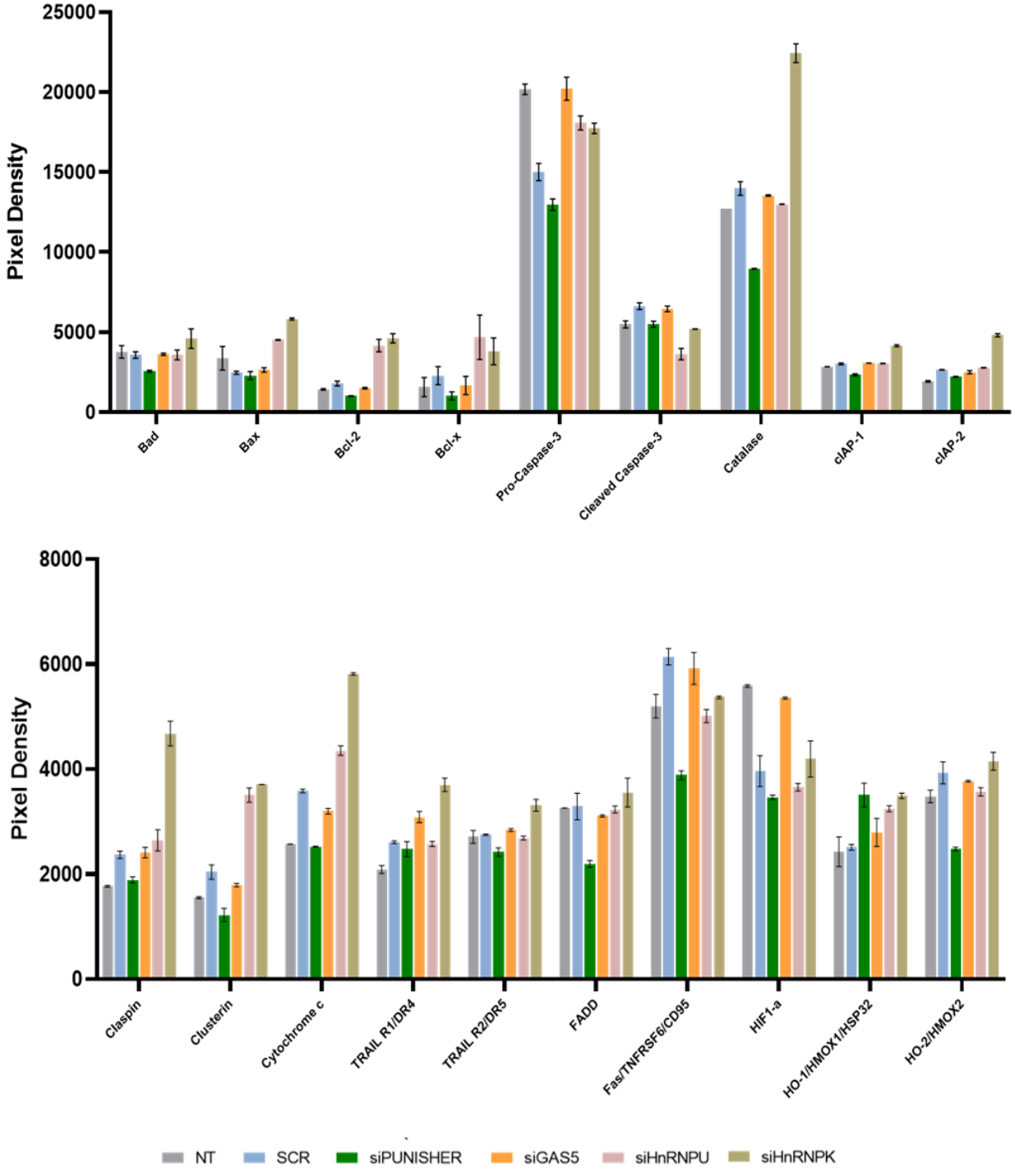
Pixel Density
25000
20000
15000
10000
5000
0
Bad
Bax
Bcl-2
Bcl-x
Pro-Caspase-3
Cleaved Caspase-3
Catalase
cIAP-1
cIAP-2
Pixel Density
8000
6000
4000
2000
0
Claspin
Clusterin
Cytochrome c
TRAIL R1/DR4
TRAIL R2/DR5
FADD
Fas/TNFRSF6/CD95
HIF1-a
HO-1/HMOX1/HSP32
HO-2/HMOX2
NT
SCR
siPUNISHER
siGAS5
siHnRNPU
siHnRNPK

OM part2

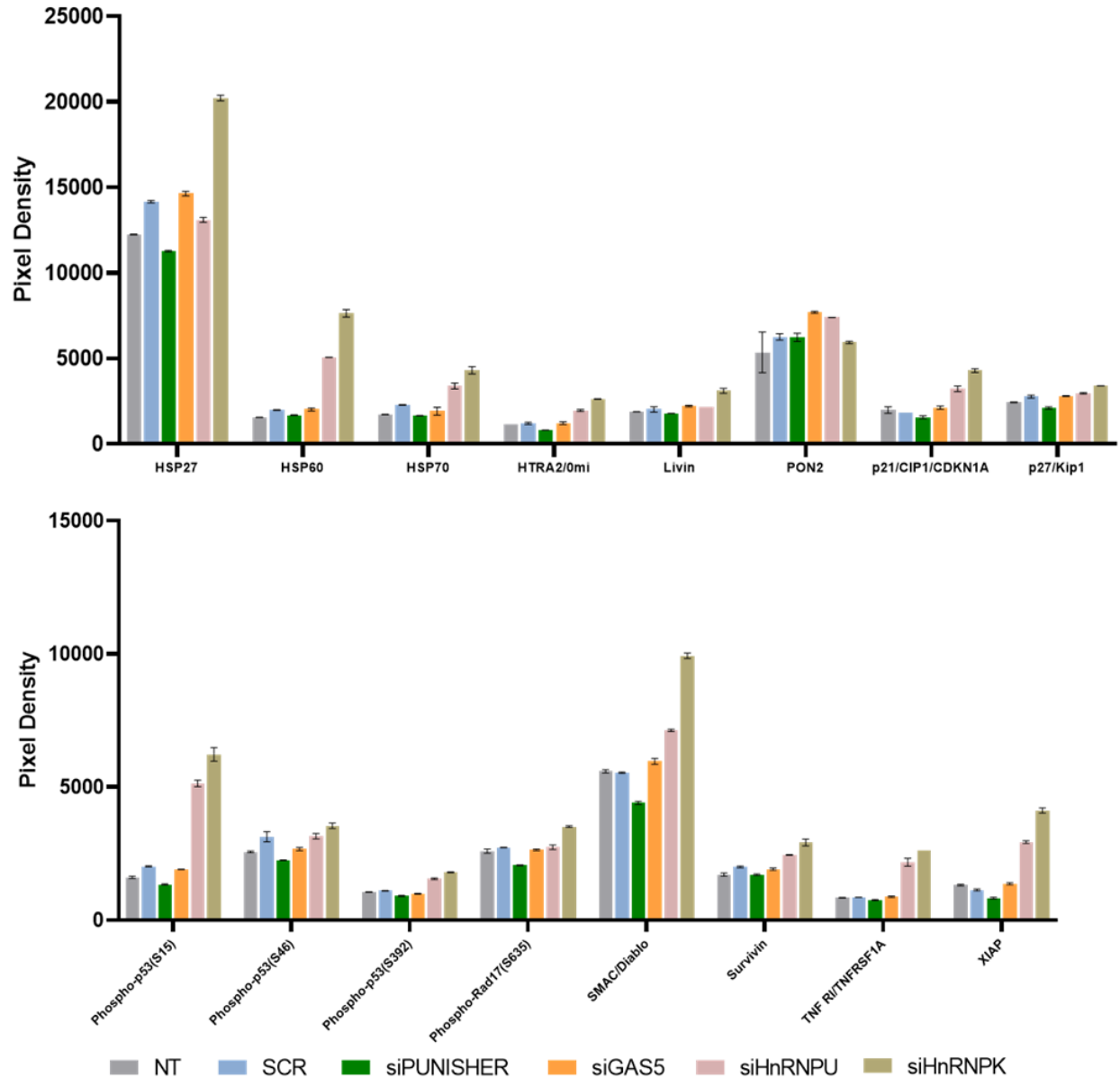
Pixel Density
25000
20000
15000
10000
5000
0
HSP27
HSP60
HSP70
HTRA2/0mi
Livin
PON2
p21/CIP1/CDKN1A
p27/Kip1
Pixel Density
15000
10000
5000
0
Phospho-p53(S15)
Phospho-p53(S46)
Phospho-p53(S392)
Phospho-Rad17(S635)
SMAC/Diablo
Survivin
TNF RI/TNFRSF1A
XIAP
NT
SCR
siPUNISHER
siGAS5
siHnRNPU
siHnRNPK

PCM part 1

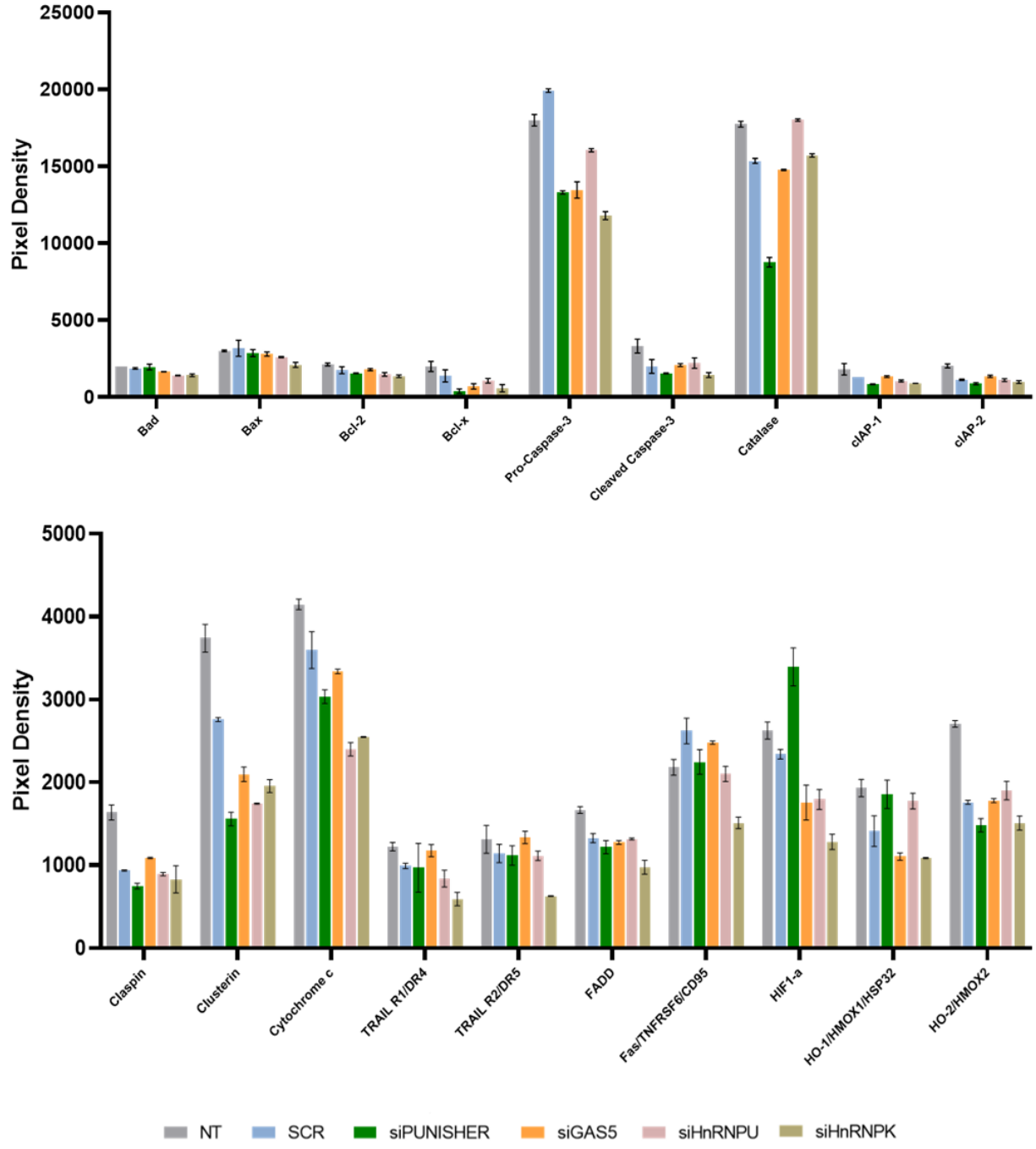
Pixel Density
25000
20000
15000
10000
5000
0
Bad
Bax
Bcl-2
Bcl-x
Pro-Caspase-3
Cleaved Caspase-3
Catalase
cIAP-1
cIAP-2
Pixel Density
5000
4000
3000
2000
1000
0
Claspin
Clusterin
Cytochrome c
TRAIL R1/DR4
TRAIL R2/DR5
FADD
Fas/TNFRSF6/CD95
HIF1-a
HO-1/HMOX1/HSP32
HO-2/HMOX2
NT
SCR
siPUNISHER
siGAS5
siHnRNPU
siHnRNPK

PCM part2

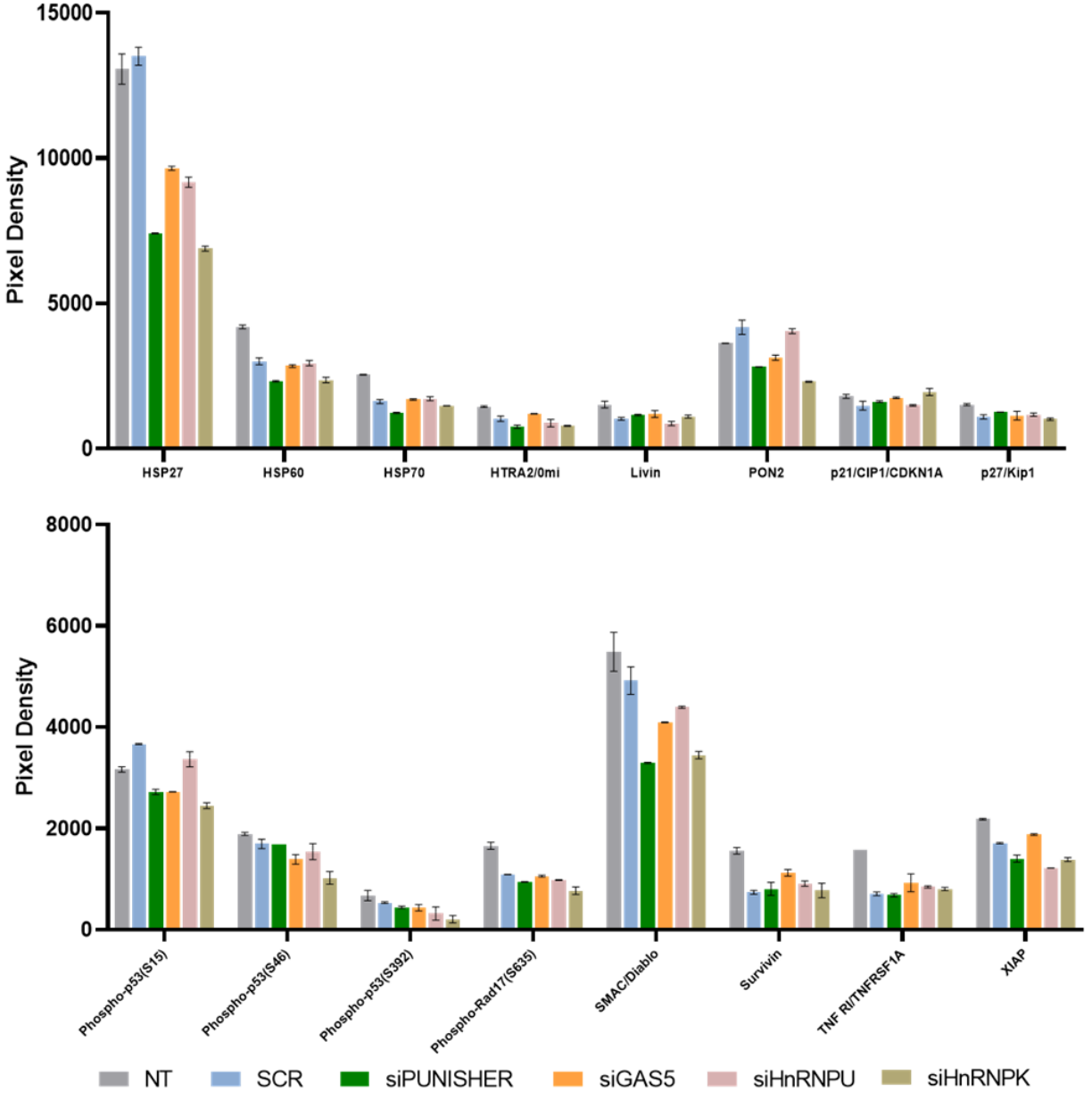
15000
10000
5000
0
Pixel Density
HSP27
HSP60
HSP70
HTRA2/0mi
Livin
PON2
p21/CIP1/CDKN1A
p27/Kip1
8000
6000
4000
2000
0
Pixel Density
Phospho-p53(S15)
Phospho-p53(S46)
Phospho-p53(S392)
Phospho-Rad17(S635)
SMAC/Diablo
Survivin
TNF RI/TNFRSF1A
XIAP
NT
SCR
siPUNISHER
siGAS5
siHnRNPU
siHnRNPK

Figure 11: Quantitative Analysis of Apoptotic Protein Expression in VICs Treated with Osteogenic Medium (OM) and pro-calcifying medium (PCM). The bar chart illustrates the pixel density quantification of apoptosis-related proteins, indicating the response of VICs to gene knockdown under different conditions. The treatments include non-treated (NT), scrambled siRNA control (SCR), and siRNA targeting PUNISHER (siPUNISHER), GAS5 (siGAS5), hnRNPU (siHnRNPU), and hnRNPK (siHnRNPK).

4. Discussion

CAVD is a complex condition involving inflammatory reactions, abnormal lipid metabolism, and the regulation of non-coding RNA. These different members merge together and thus contribute to the progress of aortic valve calcification.The classical mechanism of local inflammatory reactions and lipid metabolism abnormalities is of great significance in the occurrence and development of CAVD. Nevertheless, the past years has seen ever seriously more CAVD studies. It appears that non-coding RNA is playing an increasingly important role in the pathogenesis and progression of CAVD(Goody, et al., 2020). MiRNAs and lncRNAs are involved in various biological processes, including the transmission of regulatory signals and molecular signaling pathways (Matouk et al., 2013 and Hadji et al. 2016).

LncRNAs are now known to play crucial roles in the pathogenesis of CAVD. Dysregulation of these LncRNAs has been closely associated with the initiation and progression of CAVD. So we thought of diagnosing CAVD by identifying specific RNAs signature. Initially, targeting LncRNAs as therapeutic targets in treating CAVD may be an attractive prospect with a variety of clinical applications (Ni et al., 2018). Specifically, we investigated the roles of two lncRNAs, GAS5 and PUNISHER, in CAVD progression. These lncRNAs were selected based on our RNA sequencing data and prior evidence of their involvement in CVD. GAS5 is known for its regulatory functions in cell growth and apoptosis (Wang et al., 2016), while PUNISHER is implicated in vascular cell dysfunction and apoptosis processes (Yang et al., 2022; Hosen et al., 2021). Considering the complexity of CAVD, which involves critical processes such as calcification and EndMT, we used multiple cell models to capture the cellular heterogeneity of the disease and to understand the influence of these lncRNAs across various cellular environments (Towler, 2013).

By employing knockdown experiments, we directly assessed the impact of GAS5 and PUNISHER on key pathological processes and signaling pathways underlying CAVD. This approach was instrumental in establishing a causal link between these LncRNAs and the modulation of cellular behaviors central to the disease, such as osteogenic differentiation in VICs and the transition of endothelial cells through EndMT. Comprehensive analysis was designed to provide a holistic understanding of GAS5 and

PUNISHER's roles in CAVD, paving the way for potential therapeutic strategies targeting these LncRNAs to mitigate the disease's progression.

According to our study, we found that GAS5 and PUNISHER play similar yet distinct roles in contributing to the EndMT process and calcification, which is one reason for their significant but similar presence during CAVD progression.

To align our study with the unique processes of CAVD, we initially used VECs as a primary model to better replicate the disease-affected cellular environment. However, owing to time constraints and technical challenges associated with culturing VECs, we opted for HCAECs as an alternative model. HCAECs have functional and structural properties similar to those of VECs, making them suitable for studies involving migration arrays and EndMT (Mimouni et al., 2023). In HCAECs, knockdown of PUNISHER and GAS5 led to reduced cell proliferation and migration. Following TNFα-induced EndMT stimulation, the expression of PUNISHER and GAS5 was significantly upregulated, confirming their potential involvement in the EndMT process. Subsequent knockdown of PUNISHER and GAS5 resulted in a significant decrease in ALPL expression, indicating partial inhibition of EndMT (Hortells et al., 2018). These findings suggest that both PUNISHER and GAS5 inhibit endothelial cell migration and proliferation, implying their potential roles in promoting endothelial changes during the progression of CAVD.

In our study of CAVD, after conducting treatment for calcification, both GAS5 and PUNISHER showed increased expression in HCASMCs and VICs, indicating their significant involvement in the disease’s progression. The use of HCASMCs and VICs provides valuable insights into their similar functional and structural properties in response to calcific stimuli (Latif et al., 2007), enabling a comprehensive examination of the calcification processes in both vascular and valvular environments.

To evaluate calcification, we used common osteogenic markers, including BMP2, RUNX2, and MGP, which are well-established indicators of calcification (Shao et al., 2010). The effectiveness of our calcification models was validated by the increased expression of these markers in HCASMCs and VICs. This progression reflects the pathophysiological process of calcification, in which smooth muscle cells undergo phenotypic changes similar to those observed in valve interstitial cells, suggesting shared molecular mechanisms.

Upon the knockdown of GAS5 and PUNISHER, we observed a significant reduction in BMP2, RUNX2, and MGP expression in HCASMCs after calcification stimulation, highlighting the critical role of these lncRNAs in promoting calcification. Similarly, in VICs treated with the OM protocol, a decrease in MGP and BMP2 expression was observed, with the reduction being more pronounced in the GAS5 knockdown group. These results underscore the roles of GAS5 and PUNISHER in modulating calcification in both cell types, further supporting their contributory roles in the disease progression. Furthermore, we included knockdown groups for HNRNPU and HNRNPK due to their potential as subsequent target in the process to enhance understanding of this protein regulatory network (Hosen et al., 2021).

We used an osteogenesis-related gene detection kit to assess the impact of PUNISHER and GAS5 knockdown on calcification pathways in VICs. This analysis identified key changes in the gene expression associated with osteogenesis following lncRNA knockdown and subsequent calcification stimulation. After PUNISHER knockdown, genes such as TGFBR1, BMP2, and VEGFA were significantly downregulated, whereas ALPL and VEGFB were notably upregulated. GAS5 knockdown led to the downregulation of TGFB3, IGF1R, and COL15A1, while BMP2 and COL4A4 were significantly upregulated. These findings suggest that PUNISHER and GAS5 modulate the expression of genes involved in VIC calcification, influencing osteogenic activity during disease progression.

The results from the osteogenesis-related gene detection kit based on RT-qPCR array analysis, align with the protein-level findings from our calcification experiments. The qPCR array revealed significant changes in the expression of osteogenesis-related genes in VICs following the knockdown of GAS5 and PUNISHER, including the downregulation of TGFBR1 and BMP2.

Both PUNISHER and GAS5 were found to be instrumental in the calcification process, particularly evident in VICs, where their upregulation appears to promote osteogenic differentiation. This effect is likely mediated through the enhancement of osteogenic markers, such as RUNX2 and ALPL, signifying their active participation in driving the pathological calcification characteristic of CAVD (Nehl et al., 2023). Moreover, their involvement extends to influencing the EndMT process, crucial for the progression of valvular disease.

Our study demonstrates that the lncRNAs PUNISHER and GAS5 are significantly involved in multiple pathological processes in CAVD. Notably, we observed increased expression of these lncRNAs in calcified HCASMCs and VICs, suggesting an association with disease progression. Knockdown of these lncRNAs reduced the expression of osteogenic markers, such as RUNX2, BMP2, and MGP, indicating their role in facilitating calcification processes within these cells. In endothelial cells, PUNISHER and GAS5 knockdown decreased mesenchymal marker expression following EndMT, implying their involvement in endothelial changes that contribute to CAVD progression. Additionally, proteomic and osteogenic gene array analyses of calcified VICs revealed alterations in apoptosis-related pathways and osteogenesis-associated genes, respectively, highlighting the role of these lncRNAs in regulating both cell death and osteogenic differentiation during CAVD progression.

Overall, PUNISHER and GAS5 play crucial roles in promoting calcification, modulating EndMT, and influencing apoptosis, which underlines their significance in the pathogenesis of CAVD (Driscoll et al., 2021). These findings support the potential of targeting these lncRNAs for therapeutic intervention in CAVD.

While our study reveals the critical roles that GAS5 and PUNISHER play in the development of CAVD, it is important to be aware of the limitations inherent in our research and to suggest where future work can take us.

An important limitation of our research is that it was conducted in cell culture. Cell models offer valuable insights into molecular and cellular mechanisms but they do not exactly replicate the complex in vivo environment. In vivo, multiple cell types interact within the extracellular matrix and are influenced by systemic factors (Bogdanova et al., 2022). Although our results with HCASMCs, VICs, and HCAECs are informative, they may not fully reflect the pathophysiology of CAVD in vivo (Bartsch et al., 2021). Future studies could benefit from incorporating animal models or organ-on-a-chip technologies to better capture the systemic and multicellular nature of this disease (Mendoza et al., 2022).

A further limitation is the specificity and potential off-target effects of the RNA knockdown strategy.

Though we have observed changes in cellular behavior and marker expression following GAS5, PUNISHER knockdown, as with any other pharmacologic approach it is technically

possible that off-target effects may have interfered at some point or another to affect what we saw. Advances in gene editing technologies such as CRISPR/Cas9 offer more precise methods of manipulating genes, and may offer a clearer insight into the precise roles that these LncRNAs play(Doudna et al., 2014)..

For future research, it is of great value to know how GAS5 and PUNISHER exercise their influence in impacting on CAVD and exactly what techniques do they use.It could mean examining all the microRNA actors known to take up roles in CAVD and finding out how miR-22, miR-34c, miR-214 influence (as examples) respectively impact endothelial dysfunction, smooth muscle cell phenotypic switch and osteogenic differentiation (Yang et al., 2022; Yang et al., 2020; Li et al., 2020).

Additionally, examining the interactions between these lncRNAs and key signaling proteins within the BMP2 and RUNX2 pathways could help elucidate their mechanistic roles in CAVD progression. Given the well-established roles of BMP2 and RUNX2 in promoting osteoblastic differentiation and calcification, GAS5 and PUNISHER may modulate the expression or activity of these transcription factors, either indirectly through miRNA regulation or directly by influencing upstream signaling pathways. Specifically, PUNISHER and GAS5 may affect SMAD signaling, a downstream mediator of BMP2 (Nohe et al., 2002), thereby modulating the osteogenic differentiation of VICs. Additionally, GAS5 might regulate Wnt/β-catenin signaling, a key pathway involved in osteoblast differentiation (Day et al., 2005).

However, the regulatory roles of these lncRNAs in EndMT require further investigation. PUNISHER and GAS5 may modulate the TGF-β/SMAD pathway, which is crucial for EndMT initiation (Pardali et al., 2017). Alternatively, PUNISHER and GAS5 may influence Notch signaling, which plays a dual role in promoting and inhibiting EndMT depending on the cellular context (Kovacic et al., 2012), highlighting the complexity of these signaling interactions in disease progression.

Furthermore, treatment of these LncRNAs plays a vital role for the future of mealopiving. Such strategies as small molecule inhibitors, amoracrin hydrochloride or possibly other RNA therapies might offer patients modulation to avert the procession of disease discovered in this study. Establishing these methods will be based on a thorough

understanding of the functioning of GAS5 and PUNISHER in CAVD. This places us closer to a personalised approach for treatment of this painful ailment.

In conclusion, our work opens up new lines of enquiry into the multifaceted roles LncRNAs play in CAVD and lays a foundation for innovative diagnostic and therapeutic strategies. Building on these findings, future research can explore the molecular interactions and pathways in which GAS5 and PUNISHER take part to push the boundaries of cardiac research and bring us closer to treatments that work for the sufferers of CAVD.

5. Summary

Our investigation not only reinstalls the complexity of CAVD, a disease influenced by genetic, molecular and environmental factors but also points out the role played by LncRNAs in disease progression. The pursuit of understanding calcific aortic valvular disease, this time around has ventured into the rather little known domain LncRNAs for example GAS5 and PUNISHER. Our findings illustrate that GAS5 and PUNISHER are significantly up-regulated under CAVD-mimeking conditions, especially in human coronary artery smooth muscle cells (HCASMCs), valvular interstitial cells (VICs), and human coronary artery endothelial cells (HCAECs). Through a series of careful in vitro experiments, we showed that they contributed to key processes suggested by theories of CAVD pathogenic development, such as cell proliferation, migration, osteogenic differentiation of cells, and endothelial-to-mesenchymal transition (EndMT). More importantly, when GAS5 and PUNISHER were knocked down, not only did these pathological processes stop in short order but markers for calcification and EndMT also decreased significantly, suggesting that they might serve as targets in the treatment of this disease.

Moreover, through the application of proteome profiler array analysis and assays for detecting apoptosis or necrosis pathways as well as osteogenesis-related genes, we provided new insight into downstream effects from manipulating GAS5 and PUNISHER: variations in apoptosis or necrosis pathways, and changes of several osteogenesis-related genes' expression. These findings throw further light on the molecular mechanisms of CAVD and damn the foundations for future therapeutic interventions which alter the activity of these LncRNAs.

As we conclude, it is incumbent upon us to recognize the limitations inherent to in vitro studies and the need for further in vivo research to confirm our findings. The investigation of GAS5 and PUNISHER in clinical specimens, and their value as biomarkers to diagnose CAVD or predict prognosis is a promising subject for future study.

We hope that these discoveries will spur further investigation, with the ultimate objective that novel diagnostic and therapeutic methods are developed. And that these will eventually benefit sufferers in their fight against CAVD.

6. List of Figures

Figure 1: Structural organization of aortic valves 8

Figure 2: Schematic representation of the pathophysiological mechanisms involved in calcific aortic valvular disease (CAVD) 13

Figure 3: Impact of LncRNAs dysregulation on HCAECs after EndMT and knockdown 27

Figure 4: Endothelial-to-Mesenchymal transition and cellular responses in HCAECs following TNFα induction and LncRNAs knockdown 29

Figure 5: Impact of PUNISHER and GAS5 knockdown on calcification pathways in HCASMCs 32

Figure 6: Scratch Assay of HCASMCs migration post-siRNA treatment 33

Figure 7: Impact of PUNISHER and GAS5 knockdown on calcification markers and cell viability in VICs 35

Figure 8: BrdU incorporation assay results in VICs 36

Figure 9: Differential Gene Expression in VICs post-knockdown and calcification treatment of PUNISHER and GAS5 38

Figure 10: Proteome Profiler of apoptotic pathways activation in VICs post LncRNAs knockdown 40

Figure 11: Quantitative analysis of apoptotic protein expression in VICs treated with Osteogenic Medium (OM) and pro-calcifying medium (PCM) 41

7. List of Tables

Table 1: Information of key resources 14

8. References

Boström KI, Rajamannan NM, Towler DA. The regulation of valvular and vascular sclerosis by osteogenic morphogens. Circ Res. 2011;109(5):564-577.

Byon CH, Javed A, Dai Q, et al. Oxidative stress induces vascular calcification through modulation of the osteogenic transcription factor Runx2 by AKT signaling. J Biol Chem. 2008;283(22):15319-15327.

Caira FC, Stock SR, Gleason TG, et al. Human degenerative valve disease is associated with up-regulation of low-density lipoprotein receptor-related protein 5 receptor-mediated bone formation. J Am Coll Cardiol. 2006;47(8):1707-1712.

Carabello BA, Paulus WJ. Aortic stenosis. The lancet. 2009;373(9667):956-966.

Chen YT, Lai CF, Lin CH, Gu J, Hung CT, Yang KC. Plasma Long Noncoding RNA Lnc-CRF Predicts Adverse Cardiovascular Outcomes in Uremic Patients. In: NEPHROLOGY DIALYSIS TRANSPLANTATION. OXFORD UNIV PRESS, GREAT CLARENDON ST, OXFORD OX2 6DP, ENGLAND; 2017; Vol. 32.

Chester, Adrian, Ismail El-Hamamsy3, Jonathan T. Butcher4, Najma Latif1,2, Sergio Bertazzo5 and Magdi H. Yacoub. The living aortic valve: from molecules to function. Glob. Cardiol. Sci. Pract. 2014, 52–77.

Chung J, Kim KH, Lee SC, An SH, Kwon K. Ursodeoxycholic Acid (UDCA) Exerts Anti-Atherogenic Effects by Inhibiting Endoplasmic Reticulum (ER) Stress Induced by Disturbed Flow. Mol Cells. 2015 Oct;38(10):851-858.

Day, T. F., Guo, X., Garrett-Beal, L., & Yang, Y. (2005). Wnt/β-catenin signaling in mesenchymal progenitors controls osteoblast and chondrocyte differentiation during vertebrate skeletogenesis. Developmental cell, 8(5), 739-750.

Deck, J. D. Endothelial cell orientation on aortic valve leaflets. Cardiovasc. Res. 20, 760–767 (1986).

Doudna, J. A., & Charpentier, E. (2014). The new frontier of genome engineering with CRISPR-Cas9. Science, 346(6213), 1258096.

Driscoll, K., Cruz, A. D., & Butcher, J. T. (2021). Inflammatory and biomechanical drivers of endothelial-interstitial interactions in calcific aortic valve disease. Circulation research, 128(9), 1344-1370.

Engreitz JM, Haines JE, Perez EM, et al. Local regulation of gene expression by lncRNA promoters, transcription and splicing. Nature. 2016;539(7629):452-455.

Fernández Esmerats, J., Heath, J. & Jo, H. Shear-sensitive genes in aortic valve endothelium. Antioxid. Redox Signal. 25, 401–414 (2016).

Fu XD. Non-coding RNA: a new frontier in regulatory biology. Natl Sci Rev. 2014;1(2):190-204.c

Garikipati VNS, Verma SK, Cheng Z, et al. Circular RNA CircFndc3b modulates cardiac repair after myocardial infarction via FUS/VEGF-A axis. Nat Commun. 2019;10(1):4317.

Goody PR, Hosen MR, Christmann D, et al. Aortic valve stenosis: from basic mechanisms to novel therapeutic targets. Arterioscler Thromb Vasc Biol. 2020;40(4):885-900.

Goustin AS, Thepsuwan P, Kosir MA, Lipovich L. The Growth-Arrest-Specific (GAS)-5 Long Non-Coding RNA: A Fascinating lncRNA Widely Expressed in Cancers. Noncoding RNA. 2019 Sep 17;5(3):46.

Hadji F, Boulanger MC, Guay SP, et al. Altered DNA methylation of long noncoding RNA H19 in calcific aortic valve disease promotes mineralization by silencing NOTCH1. Circulation. 2016;134(23):1848-1862.

Hjortnaes J, Shapero K, Goettsch C, Hutcheson JD, Keegan J, Kluin J, Mayer JE, Bischoff J, Aikawa E. Valvular interstitial cells suppress calcification of valvular endothelial cells. Atherosclerosis. 2015 Sep;242(1):251-260.

Hortells, L., Sur, S., & St. Hilaire, C. (2018). Cell phenotype transitions in cardiovascular calcification. Frontiers in cardiovascular medicine, 5, 27.

Hosen MR, Goody PR, Zietzer A, Nickenig G, Jansen F. MicroRNAs as master regulators of atherosclerosis: from pathogenesis to novel therapeutic options Antioxid Redox Signal 2020; 33: 621-644.

Hosen MR, Li Q, Liu Y, Zietzer A, Maus K, Goody P, Uchida S, Latz E, Werner N, Nickenig G, Jansen F. CAD increases the long noncoding RNA PUNISHER in small extracellular vesicles and regulates endothelial cell function via vesicular shuttling. Mol Ther Nucleic Acids. 2021; 25:388-405.

Huang CK, Kafert-Kasting S, Thum T. Preclinical and clinical development of noncoding RNA therapeutics for cardiovascular disease. Circ Res. 2020;126(5):663-678.

Hutcheson, J. D., Aikawa, E., & Merryman, W. D. (2014). Potential drug targets for calcific aortic valve disease. Nature Reviews Cardiology, 11(4), 218-231.

Im Cho, K., Sakuma, I., Sohn, I. S., Jo, S. H., & Koh, K. K. (2018). Inflammatory and metabolic mechanisms underlying the calcific aortic valve disease. Atherosclerosis, 277, 60-65.

Jansen F, Wang H, Przybilla D, Franklin BS, Dolf A, Pfeifer P, Schmitz T, Flender A, Endl E, Nickenig G. Vascular endothelial microparticles-incorporated microRNAs are altered in patients with diabetes mellitus. Cardiovasc Diabetol 2016; 15: 49.

Jiang X, Ning Q. The mechanisms of lncRNA GAS5 in cardiovascular cells and its potential as novel therapeutic target. J Drug Target. 2020 Dec;28(10):1012-1017.

Javed A, Bae JS, Afzal F, Gutierrez S, Pratap J, Zaidi SK, Lou Y, van Wijnen AJ, Stein JL, Stein GS, Lian JB. Structural coupling of Smad and Runx2 for execution of the BMP2 osteogenic signal. J Biol Chem. 2008 Mar 28;283(13):8412-22.

Kovacic, J. C., Mercader, N., Torres, M., Boehm, M., & Fuster, V. (2012). Epithelial-to-mesenchymal and endothelial-to-mesenchymal transition: from cardiovascular development to disease. Circulation, 125(14), 1795-1808.

Larsson SC, Wolk A, Håkansson N, et al. Overall and abdominal obesity and incident aortic valve stenosis: two prospective cohort studies. Eur Heart J. 2017;38(28):2192-2197. doi:10.1093/eurheartj/ehx140.

Latif, N., Sarathchandra, P., Thomas, P. S., Antoniw, J., Batten, P., Chester, A. H., ... & Yacoub, M. H. (2007). Characterization of structural and signaling molecules by human valve interstitial cells and comparison to human mesenchymal stem cells. Journal of Heart Valve Disease, 16(1), 56

Latif, N., Sarathchandra, P., Chester, A. H. & Yacoub, M. H. Expression of smooth muscle cell markers and co-activators in calcified aortic valves. Eur. Heart J. 36, 1335–1345 (2015).

Lee, J. et al. A microfluidic cardiac flow profile generator for studying the efect of shear stress on valvular endothelial cells. Lab Chip 18, 2946–2954 (2018).

Lindman BR, Clavel MA, Mathieu P, et al. Calcific aortic stenosis. Nat Rev Dis Primer. 2016;2(1):1-28.

Li N, Bai Y, Zhou G, Ma Y, Tan M, Qiao F, Li X, Shen M, Song X, Zhao X, Liu X, Xu Z. miR-214 Attenuates Aortic Valve Calcification by Regulating Osteogenic Differentiation of Valvular Interstitial Cells. Mol Ther Nucleic Acids. 2020 Oct 15; 22:971-980.

Li Y, Geng Y, Zhou B, Wu X, Zhang O, Guan X, Xue Y, Li S, Zhuang X, Zhou J, Chang M, Miao G, Wang L. Long Non-coding RNA GAS5 Worsens Coronary Atherosclerosis Through MicroRNA-194-3p/TXNIP Axis. Mol Neurobiol. 2021 Jul;58(7):3198-3207.

Liu L, An X, Li Z, et al. The H19 long noncoding RNA is a novel negative regulator of cardiomyocyte hypertrophy. Cardiovasc Res. 2016;111(1):56-65.

MacGrogan D, Münch J, de la Pompa JL. Notch and interacting signalling pathways in cardiac development, disease, and regeneration. Nat Rev Cardiol. 2018;15(11):685-704.

Mathieu P, Boulanger MC, Bouchareb R. Molecular biology of calcific aortic valve disease: towards new pharmacological therapies. Expert Rev Cardiovasc Ther. 2014;12(7):851-862.

Matouk I, Raveh E, Ohana P, et al. The increasing complexity of the oncofetal h19 gene locus: functional dissection and therapeutic intervention. Int J Mol Sci. 2013;14(2):4298-4316. Published 2013 Feb 21. doi:10.3390/ijms14024298.

Ma X, Zhao D, Yuan P, Li J, Yun Y, Cui Y, Zhang T, Ma J, Sun L, Ma H, Zhang Y, Zhang H, Zhang W, Huang J, Zou C, Wang Z. Endothelial-to-Mesenchymal Transition in Calcific Aortic Valve Disease. Acta Cardiol Sin. 2020 May;36(3):183-194.

Mendoza, M., Chen, M. H., Huang, P., & Mahler, G. J. (2022). Shear and endothelial induced late-stage calcific aortic valve disease-on-a-chip develops calcium phosphate mineralizations. Lab on a Chip, 22(7), 1374-1385.

Militello, G., Weirick, T., John, D., Döring, C., Dimmeler, S., & Uchida, S. (2017). Screening and validation of lncRNAs and circRNAs as miRNA sponges. Briefings in bioinformatics, 18(5), 780-788.

Mimouni, M., Lajoix, A. D., & Desmetz, C. (2023). Experimental Models to Study Endothelial to Mesenchymal Transition in Myocardial Fibrosis and Cardiovascular Diseases. International Journal of Molecular Sciences, 25(1), 382.

Monaghan, M. G. et al. Endocardial-to-mesenchymal transformation and mesenchymal cell colonization at the onset of human cardiac valve development. Development 143, 473–482 (2016).

Moncla, L. H. M., Briend, M., Bossé, Y., & Mathieu, P. (2023). Calcific aortic valve disease: mechanisms, prevention and treatment. Nature Reviews Cardiology, 20(8), 546-559.

Nehl D, Goody PR, Maus K, Pfeifer A, Aikawa E, Bakthiary F, Zimmer S, Nickenig G, Jansen F, Hosen MR. Human and porcine aortic valve endothelial and interstitial cell isolation and characterization. Front Cardiovasc Med. 2023 Jun 20; 10:1151028.

Neph S, Vierstra J, Stergachis AB, et al. An expansive human regulatory lexicon encoded in transcription factor footprints. Nature. 2012;489(7414):83-90.

Ni WJ, Wu YZ, Ma DH, Leng XM. Noncoding RNAs in Calcific Aortic Valve Disease: A Review of Recent Studies. J Cardiovasc Pharmacol. 2018 May;71(5):317-323.

Nohe, A., Hassel, S., Ehrlich, M., Neubauer, F., Sebald, W., Henis, Y. I., & Knaus, P. (2002). The mode of bone morphogenetic protein (BMP) receptor oligomerization

determines different BMP-2 signaling pathways. Journal of Biological Chemistry, 277(7), 5330-5338.

Pardali, E., Sanchez-Duffhues, G., Gomez-Puerto, M. C., & Ten Dijke, P. (2017). TGF-β-induced endothelial-mesenchymal transition in fibrotic diseases. International journal of molecular sciences, 18(10), 2157.

Proudfoot, D., Skepper, J. N., Hegyi, L., Bennett, M. R., Shanahan, C. M., & Weissberg, P. L. (2000). Apoptosis regulates human vascular calcification in vitro: evidence for initiation of vascular calcification by apoptotic bodies. Circulation research, 87(11), 1055-1062.

Qiu, S., Adema, C. M., & Lane, T. (2005). A computational study of off-target effects of RNA interference. Nucleic acids research, 33(6), 1834-1847.

Romas E. Bone loss in inflammatory arthritis: mechanisms and therapeutic approaches with bisphosphonates. Best Pract Res Clin Rheumatol. 2005 Dec;19(6):1065-79.

Sacks, M. S., David Merryman, W. & Schmidt, D. E. On the biomechanics of heart valve function. J. Biomech. 42, 1804–1824 (2009).

Sallam T, Sandhu J, Tontonoz P. Long noncoding RNA discovery in cardiovascular disease: decoding form to function. Circ Res. 2018;122(1):155-166.

Schlotter F, Halu A, Goto S, et al. Spatiotemporal Multi-Omics Mapping Generates a Molecular Atlas of the Aortic Valve and Reveals Networks Driving Disease. Circulation. 2018; 138: 377-393.

Shao, J. S., Cheng, S. L., Sadhu, J., & Towler, D. A. (2010). Inflammation and the osteogenic regulation of vascular calcification: a review and perspective. Hypertension, 55(3), 579-592.

Shen S, Jiang H, Bei Y, Xiao J, Li X. Long non-coding RNAs in cardiac remodeling. Cell Physiol Biochem. 2017;41(5):1830-1837.

Skaria T, Bachli E, Schoedon G. WIF1 prevents Wnt5A mediated LIMK/CFL phosphorylation and adherens junction disruption in human vascular endothelial cells. J Inflamm (Lond). 2017 May 19; 14:10.

Sohmer, B. et al. Aortic valve cusp coaptation surface area using 3-dimensional transesophageal echocardiography correlates with severity of aortic valve insuficiency. J. Cardiothorac. Vasc. Anesth. 32, 344–351 (2018).

Thompson B, Towler DA. Arterial calcification and bone physiology: role of the bone–vascular axis. Nat Rev Endocrinol. 2012;8(9):529-543.

Towler DA. Molecular and cellular aspects of calcific aortic valve disease. Circ Res. 2013;113(2):198-208.

Viereck J, Thum T. Circulating Noncoding RNAs as Biomarkers of Cardiovascular Disease and Injury. Circ Res. 2017;120(2):381-399.

Wang H, Shi J, Li B, Zhou Q, Kong X, Bei Y. MicroRNA expression signature in human calcific aortic valve disease. BioMed Res Int. 2017;2017.

Wang, Y. N. Z., Shan, K., Yao, M. D., Yao, J., Wang, J. J., Li, X., ... & Yan, B. (2016). Long noncoding RNA-GAS5: a novel regulator of hypertension-induced vascular remodeling. Hypertension, 68(3), 736-748.

Xu, K. et al. Cell-type transcriptome atlas of human aortic valves reveal cell heterogeneity and endothelial to mesenchymal transition involved in calcific aortic valve disease. Arterioscler. Thromb. Vasc. Biol. 40, 2910–2921 (2020).

Xu, Y. M., Wu, D. D., Zheng, W., Yu, F. Y., Yang, F., Yao, Y., ... & Lau, A. T. (2016). Proteome profiling of cadmium-induced apoptosis by antibody array analyses in human bronchial epithelial cells. Oncotarget, 7(5), 6146.

Yang Y, Li M, Liu Y, Wang Z, Fu X, He X, Wang Q, Li XX, Ma H, Wang K, Zou L, Wang JX, Yu T. The lncRNA Punisher regulates apoptosis and mitochondrial homeostasis of vascular smooth muscle cells via targeting miR-664a-5p and OPA1. Oxid Med Cell Longev. 2022; 2022:5477024.

Yang F, Liu S, Gu Y, Yan Y, Ding X, Zou L, Xu Z, Wang G. MicroRNA-22 promoted osteogenic differentiation of valvular interstitial cells by inhibiting CAB39 expression during aortic valve calcification. Cell Mol Life Sci. 2022 Feb 21;79(3):146.

Yang L, Zhu X, Ni Y, Wu D, Tian Y, Chen Z, Li M, Zhang H, Liang D. MicroRNA-34c Inhibits Osteogenic Differentiation and Valvular Interstitial Cell Calcification via STC1-Mediated JNK Pathway in Calcific Aortic Valve Disease. Front Physiol. 2020 Aug 31; 11:829.

Yu, A. M., Choi, Y. H., & Tu, M. J. (2020). RNA drugs and RNA targets for small molecules: principles, progress, and challenges. Pharmacological reviews, 72(4), 862-898.

9. Acknowledgments

I would like to thank all those who helped me during the study in Bonn and the writing of this thesis.

I wish to express gratitude to my official supervisor, PD. Dr. med. Felix Jansen. I gratefully acknowledge the help of his supervision and his valuable suggestions during the process of my research. Importantly, I give my great appreciation to my group leader, Dr. rer. nat. Mohammed Rabiul Hosen. He is a very supportive, cheerful, and energetic researcher and gave me lots of helpful information and insightful advice at every step of my experimental process and throughout my dissertation.

I am also grateful to all the colleagues in the lab who have helped me with my research. I must express my thanks to Ms. Anna Flender, Ms. Paula Leverman and Ms. Sarah Arahouan for their assistance. Moreover, I would like to thank also Chinese scholarship committee for their financial support, which has made my project in Germany possible.

Finally, I would like to express my special thanks to my beloved parents, I will always be grateful for their love.